

Proinflammatory Signaling Regulates Hematopoietic Stem Cell Emergence

Raquel Espín-Palazón,^{1,2} David L. Stachura,^{1,4} Clyde A. Campbell,¹ Diana García-Moreno,² Natasha Del Cid,¹ Albert D. Kim,¹ Sergio Candel,² José Meseguer,² Victoriano Mulero,^{2,*} and David Traver^{1,3,*}

¹Department of Cellular and Molecular Medicine, University of California, San Diego, 9500 Gilman Drive, Natural Sciences Building 6107, La Jolla, CA 92093, USA

²Departamento de Biología Celular e Histología, Facultad de Biología, Universidad de Murcia, IMIB-Arrixaca, Campus Universitario de Espinardo, Murcia 30100, Spain

³Section of Cell and Developmental Biology, University of California, San Diego, La Jolla, CA 92093, USA

⁴Present address: Department of Biological Sciences, California State University, 400 West First Street, Chico 95929-0515 CA, USA

*Correspondence: vmulero@um.es (V.M.), dtraver@ucsd.edu (D.T.)

<http://dx.doi.org/10.1016/j.cell.2014.10.031>

SUMMARY

Hematopoietic stem cells (HSCs) underlie the production of blood and immune cells for the lifetime of an organism. In vertebrate embryos, HSCs arise from the unique transdifferentiation of hemogenic endothelium comprising the floor of the dorsal aorta during a brief developmental window. To date, this process has not been replicated *in vitro* from pluripotent precursors, partly because the full complement of required signaling inputs remains to be determined. Here, we show that TNFR2 via TNF α activates the Notch and NF- κ B signaling pathways to establish HSC fate, indicating a requirement for inflammatory signaling in HSC generation. We determine that primitive neutrophils are the major source of TNF α , assigning a role for transient innate immune cells in establishing the HSC program. These results demonstrate that proinflammatory signaling, in the absence of infection, is utilized by the developing embryo to generate the lineal precursors of the adult hematopoietic system.

INTRODUCTION

In all vertebrate animals studied, the homeostasis of adult blood and immune cells is ultimately maintained by rare subsets of hematopoietic stem cells (HSCs) (Kondo et al., 2003). During a brief window during embryonic development, these HSCs arise *de novo* from hemogenic endothelium comprising the floor of the dorsal aorta (DA) (Bertrand et al., 2010a; Boisset et al., 2010; de Bruijn et al., 2000; Kissa and Herbomel, 2010) in a process that appears to be conserved among all vertebrates (Clements and Traver, 2013; Godin and Cumano, 2002). A more complete understanding of the signaling pathways that instruct HSC emergence could in principle inform *in vitro* approaches utilizing pluripotent precursors to create patient-specific HSCs (Kyba and Daley, 2003). Despite decades of efforts, this goal has not yet been achieved, in part due to an incomplete understanding of the native molecular cues needed to establish HSC fate.

One known requirement for HSC emergence is signaling through the Notch pathway (Bigas et al., 2013). Notch regulates many forms of intercellular communication, underlying many cell-fate decisions, including key roles in embryonic patterning (Kopan and Ilagan, 2009). Although the role of Notch in the maintenance and function of adult HSCs appears to be dispensable (Bigas and Espinosa, 2012), Notch signaling is absolutely required in the embryonic specification of HSCs in both the mouse (Bigas and Espinosa, 2012) and zebrafish (Bertrand et al., 2010b). In mice, the Notch receptor Notch1 (Kumano et al., 2003) and the Notch ligand Jagged1 (Jag1) are required for HSC specification (Bigas et al., 2010). It is important to note that, because Notch signaling is also indispensable for arterial specification (Quillien et al., 2014) and because HSCs derive directly from the aortic floor, it has been difficult to distinguish whether Notch signaling regulates HSC emergence independently from its role in upstream arterial specification. Recent studies in Jag1-deficient mice have demonstrated HSC defects in the presence of normal arterial development, suggesting that these Notch requirements may be distinct and separable. Recent studies have also demonstrated that Notch signaling is required intrinsically within HSCs or their precursors (Robert-Moreno et al., 2008) via function of the Notch1 receptor (Hadland et al., 2004), suggesting that Jag1 may be a specific ligand of Notch1 in the specification of HSCs.

Tumor necrosis factor α (TNF α) is a powerful proinflammatory cytokine that plays a pivotal role in the regulation of inflammation and immunity. TNF α exerts its functions via engagement of one of two specific cell surface receptors (TNFRs), namely the 55 kDa TNFR1 (also known as TNFRSF1A) and the 75 kDa TNFR2 (also known as TNFRSF1B) (Shalaby et al., 1990). TNFR1 is expressed in most cell types, whereas TNFR2 is restricted to immune and endothelial cells (Aggarwal, 2003). Whereas TNF α signaling regulates aspects of adult hematopoiesis (Mizrahi and Askenasy, 2014), a potential role in the developmental specification of HSCs has not been addressed. However, it has been reported that TNF α and its receptors are highly expressed in the murine yolk sac and fetal liver, suggesting a possible role for this inflammatory cytokine in embryonic hematopoiesis (Kohchi et al., 1994).

Nuclear factor-kappa B (NF- κ B) is a ubiquitous, inducible transcription factor that is activated by a diverse number of stimuli, including TNF α (Ahn and Aggarwal, 2005; Brown et al., 2008). A

multitude of downstream targets, as well as upstream inducers, position NF- κ B as a general sensor of cell stress. TNF α signaling through TNFR2 is a well-known activator of NF- κ B (Aggarwal et al., 2012; Faustman and Davis, 2010). TNF α activates NF- κ B through its canonical pathway, in which I κ Bs (NF- κ B inhibitors) are phosphorylated, ubiquitinated, and degraded, releasing NF- κ B dimers that then translocate to the nucleus to bind specific NF- κ B DNA binding sites to activate gene expression (Brown et al., 2008). A direct role of NF- κ B in HSCs has not been extensively studied, although recent reports indicate that NF- κ B positively regulates the transcription of genes involved in the maintenance and homeostasis of hematopoietic stem and progenitor cells (HSPCs) (Stein and Baldwin, 2013), as well as their microenvironmental interactions (Zhao et al., 2012). Whether or not NF- κ B is important in HSC emergence has not been investigated.

TNF α and TNFRs (Tnfa and Tnfrs utilizing zebrafish nomenclature) are well conserved in all vertebrate organisms (Wiens and Glenney, 2011), and we previously demonstrated that zebrafish Tnfa interacts with Tnfr1 and Tnfr2 (Espín et al., 2013). Recent studies in the zebrafish indicate that zebrafish Tnfa functions as a proinflammatory cytokine by activating endothelial cells (Roca et al., 2008). Additionally, the genetic inhibition of Tnfrs identified an essential role for Tnfa signaling in the development and maintenance of endothelial cells (Espín et al., 2013). Because HSCs arise from hemogenic endothelial cells, we queried whether TNF signaling plays a role in HSC emergence. In the present study, we demonstrate a previously unappreciated requirement for TNF signaling in the generation of HSCs. We also show that NF- κ B is active in nascent HSCs and that this activation is essential for HSC emergence. Finally, we identify primitive neutrophils as a key source of Tnfa, assigning these cells a previously unidentified role in HSC development. In summary, we report an important role for inflammatory signaling in the birth of the adult hematopoietic system that is mediated by the proinflammatory cytokine Tnfa, the inflammatory transcription factor NF- κ B, and the Notch signaling pathway under nonpathogenic conditions.

RESULTS

Tnfa Signaling through Tnfr2 Is Required for Definitive, but Not Primitive, Hematopoiesis

We previously demonstrated that Tnfa is required for embryonic blood vessel development (Espín et al., 2013). Because HSCs are generated from arterial vessels in the embryo (Bigas et al., 2013), we investigated whether this proinflammatory cytokine also played a role in HSC development. To address this question, we isolated *kdr1*⁺ endothelial cells by fluorescence-activated cell sorting (FACS) from 26 hr postfertilization (hpf) transgenic *kdr1:mCherry* embryos and performed quantitative PCR (qPCR) for *tnfr1* and *tnfr2*. Both transcripts were enriched in these cells compared to the whole embryo (Figure S1A available online). Sorted cells expressed high levels of endogenous *kdr1* and were negative for the muscle-specific *myod* gene, demonstrating the purity of the sorted cells (Figure S1B). To investigate whether Tnfa signaling was required for HSC specification, we performed loss-of-function experiments for Tnfa and its two receptors, Tnfr1 and Tnfr2, utilizing specific antisense morpholinos (MOs) (Espín et al., 2013). In the zebrafish embryo, HSCs can be visualized

along the axial vessels by expression of *cmyb* using whole-mount in situ hybridization (WISH) (Burns et al., 2005). The number of *cmyb*⁺ cells in or near the floor of the DA was significantly reduced in Tnfa- and Tnfr2-deficient embryos compared with their wild-type (WT) siblings (Figures 1A and 1B). However, loss of Tnfr1 showed no effect on HSC number, and its simultaneous depletion with Tnfr2 was not significantly different than loss of Tnfr2 alone (Figures 1A and 1B), indicating that the action of Tnfa through Tnfr2, but not Tnfr1, is important in HSC development. This result was supported by quantitation of *cd41:eGFP*⁺ HSPCs (Bertrand et al., 2008) using flow cytometry, which were significantly decreased in Tnfr2- and Tnfa- deficient fish at 3 days postfertilization (dpf) (Figure 1C).

To further confirm the reduction of HSCs in Tnfr2- and Tnfa-deficient embryos, we directly visualized emerging HSCs from the floor of the DA in *kdr1:mCherry; cmyb:GFP* double transgenic embryos (Bertrand et al., 2010a) at 48 hpf by confocal microscopy (Figure 1D). Consistent with the results above, the number of double-positive *kdr1*⁺; *cmyb*⁺ HSCs in the floor of the DA was reduced ~50% when compared to control embryos (Figures 1D and 1E), unaffected in Tnfr1 deficient embryos, and showed a similar 50% decrease in Tnfr1+Tnfr2 double-depleted embryos (Figure S1C). These reductions could be due to a defect in the initial specification of HSCs or in their subsequent maintenance. To distinguish between these possibilities, we performed WISH for the nascent HSC marker *runx1* at earlier time points. Both Tnfr2- and Tnfa- deficient embryos showed significant reduction in the number of *runx1*⁺ cells in the aortic floor at 24, 28, and 36 hpf (Figures S1D and S1E), indicating that the functions of Tnfa and Tnfr2 are important during the earliest steps of HSC specification.

We next examined subsequent developmental stages for possible roles of Tnfa in the maintenance of nascent HSCs. To determine whether Tnf receptor expression is modulated following HSC specification, we purified *kdr1*⁺; *cmyb*⁻ endothelial cells and *kdr1*⁺; *cmyb*⁺ HSCs from 48 hpf *kdr1:mCherry; cmyb:GFP* embryos by FACS. qPCR analysis showed that, whereas *tnfr1* mRNA levels were similar in HSCs and endothelial cells, *tnfr2* transcripts markedly increased in HSCs (Figure 1F). As this result suggested that Tnfr2 may play a role in HSC maintenance, we analyzed changes in HSC number in individual embryos over time. The number of *cmyb*⁺; *kdr1*⁺ cells in WT animals expanded between 36 and 48 hpf, whereas Tnfr2- or Tnfa-deficient siblings showed similar numbers of HSCs at either time point (Figures 1G and 1H). Together, these results suggest that Tnfa signaling through Tnfr2 is important both in the first steps of HSC specification and in their subsequent maintenance following emergence from the aortic endothelium. Finally, we examined later larval stages by monitoring the expression of *rag1* and *lck*, two genes expressed in developing thymocytes (Langenau et al., 2004) because the T cell lineage derives exclusively from HSCs (Bertrand et al., 2008; Gering and Patient, 2005). Expression of *rag1* was completely or nearly absent, respectively, in Tnfr2- and Tnfa-deficient animals at 4 dpf (Figure 1I). However, the thymic anlage developed normally in all morphants, assessed by the expression of the thymic epithelial marker *foxn1* (Figure 1J). These results were further verified utilizing *lck:eGFP* transgenic animals to track T cell development (Langenau et al., 2004).

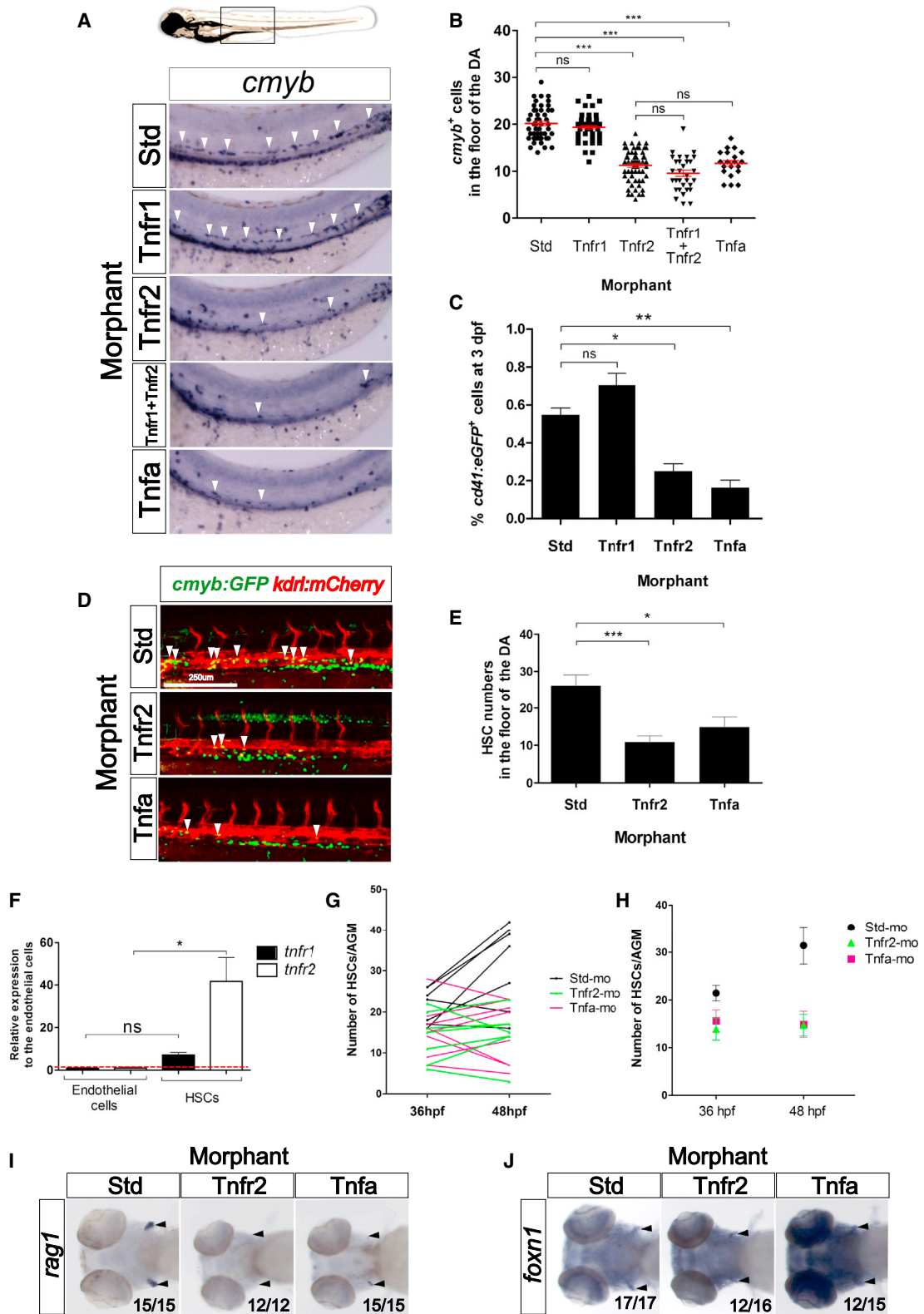


Figure 1. Tnfa and Tnfr2 Are Required for HSC Generation

(A) Standard control (Std), Tnfr1, Tnfr2, Tnfa, Tnfr1, and Tnfr2 morphants were examined by WISH for *cmyb* expression in the aortic floor at 48 hpf. White arrowheads denote *cmyb*⁺ HSPCs.

(legend continued on next page)

T cells were absent in *Tnfr2*- and *Tnfa*- deficient larvae at 4 dpf, whereas *Tnfr1*-deficient siblings showed normal T cell development (Figure S1F). Together, these results indicate that *Tnfa* signals via *Tnfr2* and that this signaling pathway is important both for early specification and subsequent maintenance of HSC fate, such that the lineage is apparently lost by 4 dpf.

To further dissect the role of *Tnfa* signaling in hematopoiesis, we assessed whether *Tnfa* and its receptors were required for the first waves of hematopoiesis, commonly referred to as “primitive” due to the transience of these cells and lack of upstream multipotent progenitors. In zebrafish, primitive hematopoiesis generates macrophages, neutrophils, and erythrocytes. The expression of *csf1ra*, a specific marker of macrophages (Herbomel et al., 2001), was unaffected in *Tnfa*-, *Tnfr1*-, and *Tnfr2*-deficient embryos at 24 hpf (Figure S1G). Additionally, primitive neutrophils were unaffected at 30 hpf, as assayed using transgenic *mpx:eGFP* animals (data not shown). Similarly, primitive erythropoiesis, assessed by expression of the erythroid-specific transcription factor *gata1a* at 24 hpf, was unaffected in morphant embryos (Figure S1G). Overall, these results indicate that *Tnfa* signaling is dispensable for primitive hematopoiesis and indispensable for definitive hematopoiesis in the zebrafish embryo.

Tnfr2- and Tnfa-Deficient Embryos Display Normal Vasculogenesis

Because HSCs originate in arterial vessels, many mutants with vascular or arterial specification defects also have hematopoietic defects (Bigas and Espinosa, 2012). No vascular abnormalities were observed in *Tnfr2*- or *Tnfa*-deficient embryos at 24 hpf when assayed by WISH for the endothelial marker *kdrl* at the MO doses used in this study (Figure 2A), and circulation was normal (*gata1:DsRed*⁺, red blood cells) but reduced numbers of HSPCs and thrombocytes (*cd41:eGFP*⁺) at 3 dpf (Figure 2B). These results suggest that the functions of *Tnfr2* and *Tnfa* are required specifically during HSC development independently of their role in developing vasculature. Thus, we could uncouple the vascular defects previously described for *Tnfr2* (Espín et al., 2013) from its effects on HSC development using lower doses of *Tnfr2* MO.

To address whether HSC defects in *Tnfr2*- and *Tnfa*-deficient animals were a consequence of impaired arterial specification, we performed WISH for the arterial markers *efnb2a*, *dlc*,

notch1b, and *notch3* (Lawson et al., 2001) in morphant embryos at 28 hpf. We observed no alterations in transcript levels when compared to control siblings (Figure 2C). Taken together, these data indicate that *Tnfa* signaling through *Tnfr2* is specifically required for HSC development.

Tnfr2 Is Intrinsically Required for HSC Development

Because *Tnfr2* is expressed in endothelial cells (Figure S1A), we hypothesized that *Tnfr2* is intrinsically required within the vascular lineage for HSC development. To test this hypothesis, we generated a transgenic zebrafish line in which the WT form of *tnfr2* is upregulated via induction of the Gal4 transcriptional transactivator. HSC development was observed by confocal microscopy following overexpression of *Tnfr2* specifically within the vasculature in *fli1a:Gal4; UAS:RFP; cmyb:GFP; UAS:tnfr2* animals. The number of RFP⁺GFP⁺ HSCs in quadruple transgenic embryos was significantly increased compared to their *Tnfr2*⁻ siblings (Figures 2D and 2E), demonstrating that *Tnfr2* activity induces or supports the HSC program following targeted expression to the vasculature.

To verify that the loss of HSCs in *Tnfr2* morphants was not due to the apoptosis of endothelial cells, we performed a TUNEL assay and immunohistochemistry for GFP in *kdrl:GFP* embryos injected with *Tnfr2* MO. Analysis of endothelial cells by confocal microscopy at 28 hpf indicated that loss of *Tnfr2* caused no increased apoptotic endothelial cells within the DA (Figure S2A), even though there was an increase in apoptotic nonendothelial cells. As a positive control for apoptosis in control animals, we imaged the lens of the eye (Cole and Ross, 2001) (Figure S2B). We also performed WISH for *runx1* in the same experiment to verify the reduction of HSCs in these embryos (Figures S2C and S2D). These results, together with the findings that there are no detectable apoptotic endothelial cells in the DA at 28 hpf (Kobayashi et al., 2014) indicate that the HSC specification defect in *Tnfr2*-deficient embryos is not caused by apoptosis induced by alterations of *Tnfr1*/*Tnfr2* ratios within the vasculature.

Tnfa Signaling Acts Upstream of Notch during HSC Specification

During Notch activation, Notch receptors are stimulated by ligands from neighboring cells, triggering the cleavage of the Notch intracellular domain (NICD), which enters the nucleus to

(B) Quantification of *cmyb*⁺ HSPCs from (A). Each dot represents total *cmyb*⁺ cells per embryo. The mean ± SEM for each group of embryos is shown in red.
 (C) *cd41:eGFP* transgenic embryos were injected with Std, *Tnfr1*, *Tnfr2*, and *Tnfa* MOs and subjected to flow cytometric analysis at 3 dpf. Each bar represents the percentage of *cd41:GFP*⁺ cells in each sample and is the mean ± SEM of three to seven independent samples of five embryos each.
 (D) Maximum projections of 48 hpf *cmyb:GFP; kdrl:mCherry* double-transgenic embryos injected with Std, *Tnfr2*, and *Tnfa* MOs. Arrowheads denote *cmyb*⁺, *kdrl*⁺ HSCs along the DA. All views: anterior to left.
 (E) Enumeration of *cmyb*⁺, *kdrl*⁺ HSCs shown in (D). Bars represent mean ± SEM of Std (n = 13), *Tnfr2* (n = 13), and *Tnfa* (n = 8) morphants.
 (F) *cmyb*⁻, *kdrl*⁺ endothelial cells and *cmyb*⁻, *kdrl*⁺ HSCs were isolated from *cmyb:GFP; kdrl:mCherry* transgenic fish by FACS at 48 hpf and examined for expression of *tnfr1* and *tnfr2*. Bars represent mean ± SEM of two biological replicates.
 (G) Confocal tracking of HSC numbers in the floor of the DA from individual *cmyb:GFP; kdrl:mCherry* transgenic animals at 36 and 48 hpf following depletion of *Tnfr2* or *Tnfa* compared to standard control morphants.
 (H) Means ± SEM of *cmyb*⁺ cell numbers from (G).
 (I and J) WISH for the T lymphocyte and thymic epithelial markers *rag1* (I) and *foxn1* (J) (black arrowheads), respectively, in *Tnfr2* and *Tnfa* morphants compared to Std controls at 4 dpf. All views are ventral, with anteriors to left. Numbers represent embryos with displayed phenotype; ns, not significant; *p < 0.05, **p < 0.01, and ***p < 0.001.
 See also Figure S1.

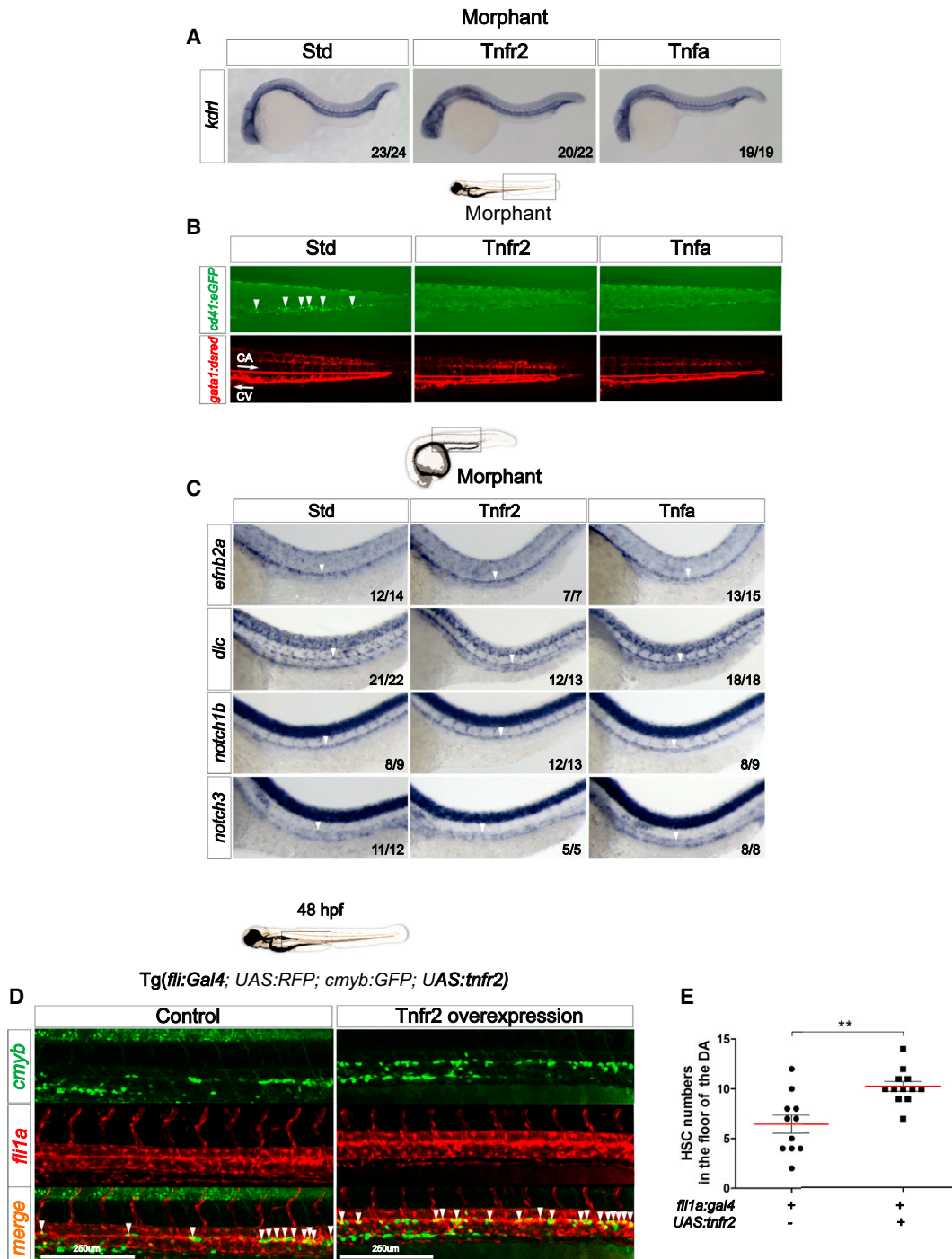


Figure 2. Signaling through Tnfr2 Regulates HSC Development Independently of Its Role in Vascular Formation

(A) Std, Tnfr2, and Tnfa morphants were interrogated by WISH for the expression of *kdr1* at 24 hpf. (B) *cd41:eGFP*; *gata1a:dsred* double-transgenic embryos were injected with Std, Tnfr2, and Tnfa MOs and visualized at 3 dpf. Arrowheads indicate *cd41:eGFP*⁺ HSPCs in the CHT located between the caudal artery (CA) and caudal vein (CV). Arrows indicate blood flow direction. (C) Expression of the arterial markers *efnb2a*, *dlc*, *notch1b*, and *notch3* in Std, Tnfr2, and Tnfa morphants analyzed by WISH at 28 hpf. Arrowheads denote the CA. (D) Maximum projections of *fl1a:Gal4*; *UAS:tnfr2*; *cmyb:GFP*; *kdr1:mCherry* transgenic embryos at 48 hpf. Region shown includes the DA, and arrowheads denote *cmyb*⁺; *kdr1*⁺ HSCs. (E) Enumeration of *cmyb*⁺; *kdr1*⁺ HSCs shown in (D). Each dot is the number of *kdr1*⁺; *cmyb*⁺ cells per embryo. Means ± SEM for each group is shown in red. **p < 0.01. All views are lateral, with anteriors to the left. Numbers in panels represent larvae with indicated phenotype. See also Figure S2.

function as transcription factor essential for cell fate decisions (Lai, 2004). There are four Notch receptors (Notch1a, 1b, 2, and 3), five Delta family ligands (Dla, Dlb, Dlc, Dld, and Dll4) and three Jagged ligands (Jagged 1a, Jagged 1b, and Jagged 2) in zebrafish. Because $\text{TNF}\alpha$ activates the Notch pathway in certain contexts (Fernandez et al., 2008; Wang et al., 2013), we queried whether signaling through Tnfr2 may similarly activate Notch signaling to specify HSCs. We performed loss-of-function experiments for Tnfr2 and Tnfa in transgenic *tp1:eGFP* animals, in which GFP is expressed by cells having recently experienced Notch signaling (Parsons et al., 2009). Consistent with our other findings, the depletion of either Tnfa or Tnfr2 led to a 2-fold reduction in *tp1:eGFP*⁺; *kdrl:mCherry*⁺ HSPCs in the aortic floor at 26 hpf (Figure 3A, arrowheads, and Figure 3B). These observations indicate that Tnfr2 signaling is upstream of Notch signaling during HSC specification.

If Notch signaling is indeed required downstream of Tnfr2 function for HSC specification, then ectopic expression of the Notch1a intracellular domain (NICD1a) should rescue the lack of HSCs in Tnfr2- and Tnfa-deficient embryos. We performed two different experiments to address the timing and tissue specificity of this Tnfa-dependent Notch requirement. To provide temporal control of NICD1a induction, we utilized inducible *hsp70:Gal4*; *UAS:NICD1a-myc* double-transgenic embryos, which express NICD1a under the control of the inducible Gal4 system. Induction of NICD1a at 18 hpf rescued the depletion of *runx1*⁺ HSCs at 28 hpf along the DA in both Tnfa and Tnfr2 morphants (Figure 3C). We then enforced the expression of NICD1a within endothelial cells utilizing *kdrl:Gal4*; *UAS:NICD1a-myc* double-transgenic embryos that had been injected with Tnfr2 or Tnfa MOs. Endothelial expression of NICD1a restored *runx1*⁺ cells along the aortic floor (Figure 3D), indicating that TNF signaling activates the Notch pathway within hemogenic endothelium to specify HSC fate.

Tnfa Induces Jag1a within Endothelial Cells to Promote HSC Specification through Notch1a

We next investigated potential mechanisms by which Tnfa and Tnfr2 induced Notch activation. Due to the fact that Tnfa signaling has been reported to induce or inhibit the expression of specific Notch ligands (Fernandez et al., 2008; Sainson et al., 2008), we analyzed expression of the eight zebrafish Notch ligands within purified *kdrl*⁺ endothelial cells from Tnfr2-deficient embryos. Only *jag1a* expression was downregulated in Tnfr2 morphants relative to controls (Figure 4A). Using a *fli1a:Gal4* driver to enforce expression of Tnfr2 specifically within the vasculature, we examined Notch ligand expression in *fli1a:Gal4*; *UAS:tnfr2* animals by qPCR (Figure 4B). We detected a 20-fold increase of *tnfr2* in *UAS:tnfr2*⁺ compared to *UAS:tnfr2*⁻ embryos (Figure 4B). Consistent with our previous results, only *jag1a* mRNA levels were increased following the enforced expression of Tnfr2 (Figure 4B).

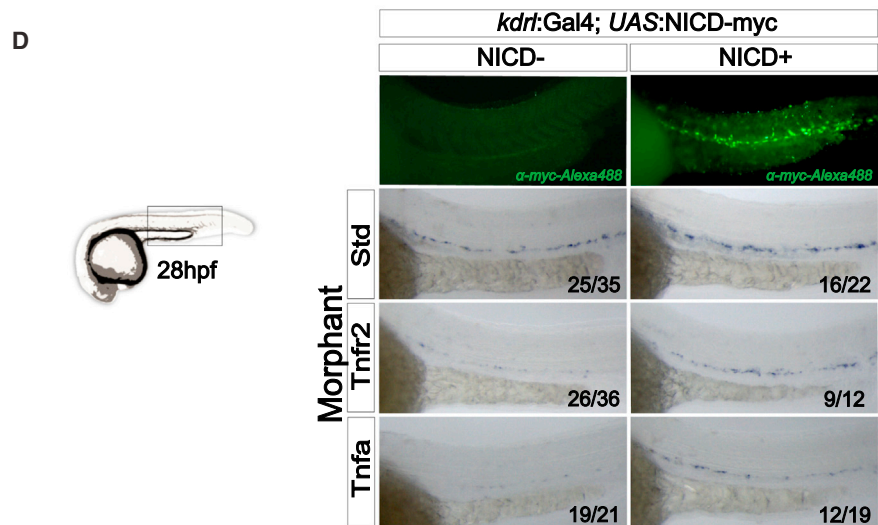
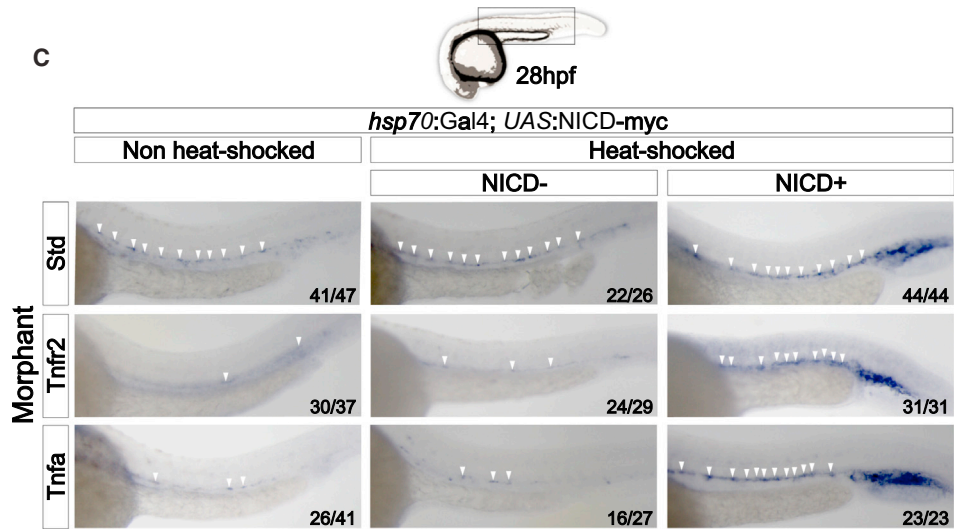
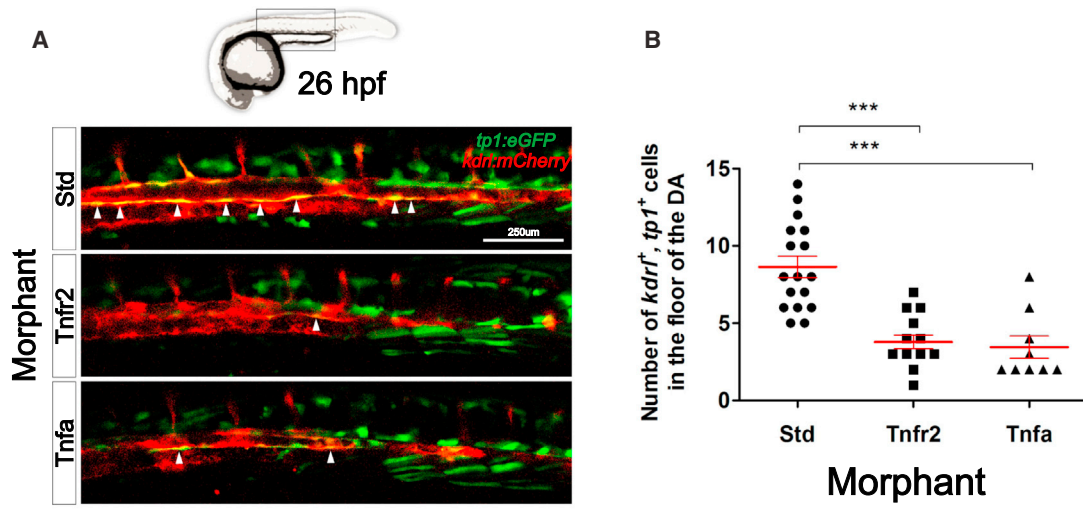
Interestingly, Jag1 is required for the generation of definitive hematopoietic cells in mice but is dispensable for arterial development. A potential role for Jag1 in zebrafish HSPC development has not been addressed. Two paralogues of the single *JAG1* human gene are present in the zebrafish genome: *jag1a* and *jag1b*. Because only *jag1a* levels were modulated by Tnfr2, we per-

formed loss-of-function experiments with this gene. Loss of *jag1a* led to decreased HSC numbers as analyzed by *runx1* expression along the DA (Figure 4C). However, specification of aortic fate was normal, as *efnb2a* and *dlc* levels were unperturbed (Figure 4C). To further verify that Tnfr2 and Jag1a were in the same genetic pathway, we performed synergy studies by coinjecting low doses of Tnfr2 and Jag1a MOs simultaneously. Aortic *runx1*⁺ cells were significantly reduced in Tnfr2- and Jag1a- double-deficient embryos compared to single-deficient embryos (Figure 4D). Tnfr2 function thus lies genetically upstream of *jag1a* during HSC specification. To investigate potential Jag1a-presenting cells, we isolated *cmyb*⁻, *kdrl*⁺ endothelial cells and *cmyb*⁺, *kdrl*⁺ HSCs for qPCR analysis of *jag1a* at 48 hpf. *jag1a* transcripts were 4-fold more abundant in endothelial cells than in HSCs (Figure S3), suggesting that Notch signaling in HSCs or hemogenic endothelium is activated by neighboring Jag1a⁺ endothelial cells.

We next investigated which of the four Notch receptors were downstream of Jag1a during HSC induction. In the mouse, Notch1 is required within HSCs or their lineal precursors to instruct HSC fate. We therefore focused upon the two zebrafish orthologs of human NOTCH1, Notch1a and Notch1b. To investigate whether either receptor functioned downstream of Tnfr2 to specify HSCs, we performed synergy experiments by coinjecting low doses of Tnfr2 MO with morpholinos against Notch1a or Notch1b. Only the simultaneous depletion of Tnfr2 and Notch1a, but not Tnfr2 and Notch1b, led to a statistically significant decrease in *runx1* expression compared to single morphants at 28 hpf (Figure 4E). This finding suggests that Notch1a serves as the Notch receptor for Jag1a to specify HSC fate downstream of Tnfr2.

The Proinflammatory Transcription Factor NF- κ B Is Active in Emerging HSCs

Activation of TNF receptors by ligand binding leads to the recruitment of adaptor proteins that trigger NF- κ B activation (Aggarwal et al., 2012). Moreover, the induction of *Jag1* transcription by Tnfa in murine endothelial cells is NF- κ B dependent (Johnston et al., 2009). Interestingly, NF- κ B (as well as Tnfr2 and Jag1) is necessary for embryonic vessel development (Santoro et al., 2007). These lines of evidence suggested that NF- κ B could have a previously unappreciated role in HSC specification, prompting us to examine its role in HSC development. We utilized an NF- κ B activation reporter transgenic line (Kanter et al., 2011) in combination with the *kdrl:mCherry* transgene to perform confocal analysis of the DA at different time points. Interestingly, we observed NF- κ B^{high} cells in the floor of the DA at 24 hpf, typically in pairs and in direct contact with each other (Figure 5A). We also observed NF- κ B⁺ cells along the roof of the DA but at a much lower frequency than in the floor (data not shown). NF- κ B⁺, *kdrl*⁺ cells remained visible at 30 hpf (Figure 5A) and underwent endothelial-to-hematopoietic transition (EHT) (Movie S1), a characteristic feature of emerging HSCs. To further evaluate whether HSCs had increased NF- κ B activation compared to their surrounding endothelial neighbors, *kdrl*⁺; *cmyb*⁺ HSCs and *kdrl*⁺; *cmyb*⁻ endothelial cells were isolated from 48 hpf *kdrl:mCherry*; *cmyb:GFP* embryos by FACS for qPCR analyses. Whereas endothelial cells had 20- to 30-fold induction of the NF- κ B response genes interleukin 1 beta



(legend on next page)

(*il1b*) and nuclear factor of kappa light polypeptide gene enhancer in B cells inhibitor alpha a (*ikbaa*) relative to whole-embryo expression, HSCs displayed 300- and 2,300-fold increases in *il1b* and *ikbaa*, respectively (Figure 5B). Immunohistochemistry for the NF- κ B subunit p65 in *kdrl:mCherry* embryos showed that, although p65 was detected in the cytoplasm of every cell as expected, it was more intense in the pronephros (Figures 5C and 5D, yellow asterisks), in the DA, and in cells potentially undergoing the endothelial to hematopoietic transition in the aortic floor (Figures 5C and 5D, arrow). These results indicate that NF- κ B activation is a characteristic feature of emerging HSCs.

Multiple lines of evidence support the integration of the Notch and NF- κ B signaling pathways during the differentiation of various cell types (Ang and Tergaonkar, 2007; Cao et al., 2011; Espinosa et al., 2010; Espinosa et al., 2003; Shin et al., 2006; Song et al., 2008). For this reason, we investigated whether NF- κ B⁺ cells in the floor of the DA also had active Notch signaling, utilizing double-transgenic *tp1:nlsCherry; NFKB:GFP* animals to simultaneously visualize respective Notch and NF- κ B activation. NF- κ B⁺ cells in the floor of the DA were also *tp1*⁺ (Figure 5E). No NF- κ B⁺, *tp1*⁻ cells were found in the floor of the DA, suggesting that Notch is (or was previously) active in NF- κ B⁺ HSPCs.

NF- κ B Activation Is Required for HSC Specification and Acts Downstream of Tnfr2

To determine whether NF- κ B function is required for HSC emergence, we developed a Tg(*UAS:dn-ikbaa*) transgenic animal that functions as a dominant-negative inhibitor of NF- κ B (Figures S4A and S4B). Similar truncation constructs have been utilized in vitro to inhibit NF- κ B activation (Abbas and Abu-Amer, 2003). At 6 hr post-heat-shock in *hsp70:Gal4; UAS:dn-ikbaa* animals, *dn-ikbaa* mRNA levels were detected in *dn-ikbaa*⁺, but not in *dn-ikbaa*⁻, siblings (Figure S4C). qPCR for the NF- κ B response gene *il1b* in FACS-purified *fli1a*⁺ endothelial cells showed significant downregulation in the *dn-ikbaa*⁺ embryos compared to their *dn-ikbaa*⁻ siblings (Figures S4D and S4E). Lipopolysaccharide (LPS) challenge of WT embryos produced a significant increase in *il1b* expression compared to PBS-injected controls, as previously described (van der Vaart et al., 2013), but not in *dn-ikbaa*⁺ embryos (Figures S4F and S4G), indicating that *dn-ikbaa*⁺ embryos are unable to trigger an inflammatory response through NF- κ B. These results thus demonstrate that *UAS:dn-ikbaa* embryos have impaired NF- κ B activation.

Blockade of NF- κ B function at 20 hpf in *hsp70:Gal4; UAS:dn-ikbaa* animals led to loss of HSCs at 48 hpf (Figure 6A). Loss of NF- κ B specifically within the vasculature using *fli1a:Gal4; UAS:dn-ikbaa* double-transgenic embryos also led to a depletion

of *cmyb*⁺ cells (Figure 6B). qPCR for *il1b* in FACS-purified endothelial cells showed a 3-fold decrease in Tnfr2 morphants (Figure 6C), demonstrating that NF- κ B acts downstream of Tnfr2 during HSC specification. Together, these results suggest that NF- κ B activation in hemogenic endothelium is a key event in the specification of HSCs.

Primitive Neutrophils Are the Key Source of Tnfa

In adult organisms, immune cells are the main source of TNF α , including T and B lymphocytes, macrophages, and neutrophils (Aggarwal, 2003). From 22 to 72 hpf, the temporal window over which zebrafish HSCs emerge from aortic endothelium, the only leukocytes present are primitive myeloid cells, namely macrophages and neutrophils (Herbomel et al., 1999; Le Guyader et al., 2008). Interestingly, *tnfa* expression in the zebrafish embryo was not detectable during the first 9 hr of development but was expressed before 24 hpf (Espín et al., 2013) when HSCs are initially specified (Clements and Traver, 2013). We therefore hypothesized that primitive myeloid cells were the source of Tnfa. We isolated *mpeg:GFP*⁺ primitive macrophages and *mpx:GFP*⁺ primitive neutrophils by FACS at two different time points and performed qPCR for *tnfa* (Figure 7A). Although both populations expressed *tnfa*, the highest expression was observed within the neutrophil fraction (Figure 7A). We then utilized a pu1 MO to specifically ablate both primitive myeloid lineages in vivo (Rhodes et al., 2005). pu1 MO efficacy was validated by WISH using the panleukocyte marker *l-plastin* and the neutrophil marker *mpx* at 48 hpf (Figure S5A). Following ablation of primitive myeloid cells in pu1 morphants, HSCs were enumerated by confocal microscopy of *kdrl*⁺*cmyb*⁺ cells. A 2-fold decrease in HSC number was detected in pu1 morphants compared to their control siblings (Figures 7B and 7C). To elucidate which primitive myeloid population was responsible for the decrease in HSC number, we utilized an irf8 MO (Li et al., 2011), which skews myeloid development to almost entirely neutrophilic. Loss of the macrophage lineage was confirmed in irf8 morphants by qPCR for the macrophage-specific marker *mpeg1* (Figure S5B). Surprisingly, the number of *kdrl*⁺; *cmyb*⁺ HSCs increased following loss of the macrophage lineage (Figures 7D and 7E). In agreement with our *tnfa* expression data, this result suggests that neutrophils are the key source of the Tnfa needed for HSC emergence. To test this hypothesis, we quantified *tnfa* expression levels in pu1- and irf8-deficient animals. Expression of *tnfa* was consistently decreased following loss of pu1 function and increased following loss of irf8 function (Figure 7F). In addition, although *runx1* was upregulated in irf8-deficient embryos, the simultaneous depletion of Tnfa and Irf8 led to a marked reduction in *runx1* expression, despite the elevated numbers of neutrophils present (Figure 7G). These

Figure 3. Tnfa and Tnfr2 Act Upstream of Notch Signaling during HSC Specification

(A) *tp1:eGFP; kdrl:mCherry* embryos injected with Std, Tnfr2, and Tnfa MOs were visualized at 26 hpf. Arrowheads indicate cells in the floor of the DA with active Notch signaling.

(B) Enumeration of *tp1*⁺, *kdrl*⁺ HSCs from (A). Each dot represents the number of HSCs per embryo, and red lines indicate means \pm SEM. ***p < 0.001.

(C) *hsp70:Gal4; UAS:NICD-myc* embryos injected with Std, Tnfr2, and Tnfa MOs were heat shocked at 18 hpf and WISH for *runx1* was performed at 28 hpf. Arrowheads denote HSCs along the DA.

(D) *kdrl:Gal4; UAS:NICD-myc* embryos injected with Std, Tnfr2, and Tnfa MOs were analyzed by WISH for *runx1* at 28 hpf. NICD⁺ larvae were identified using anti-myc-Alexa488 antibody (top). Numbers in panels represent the numbers of larvae with indicated phenotype.

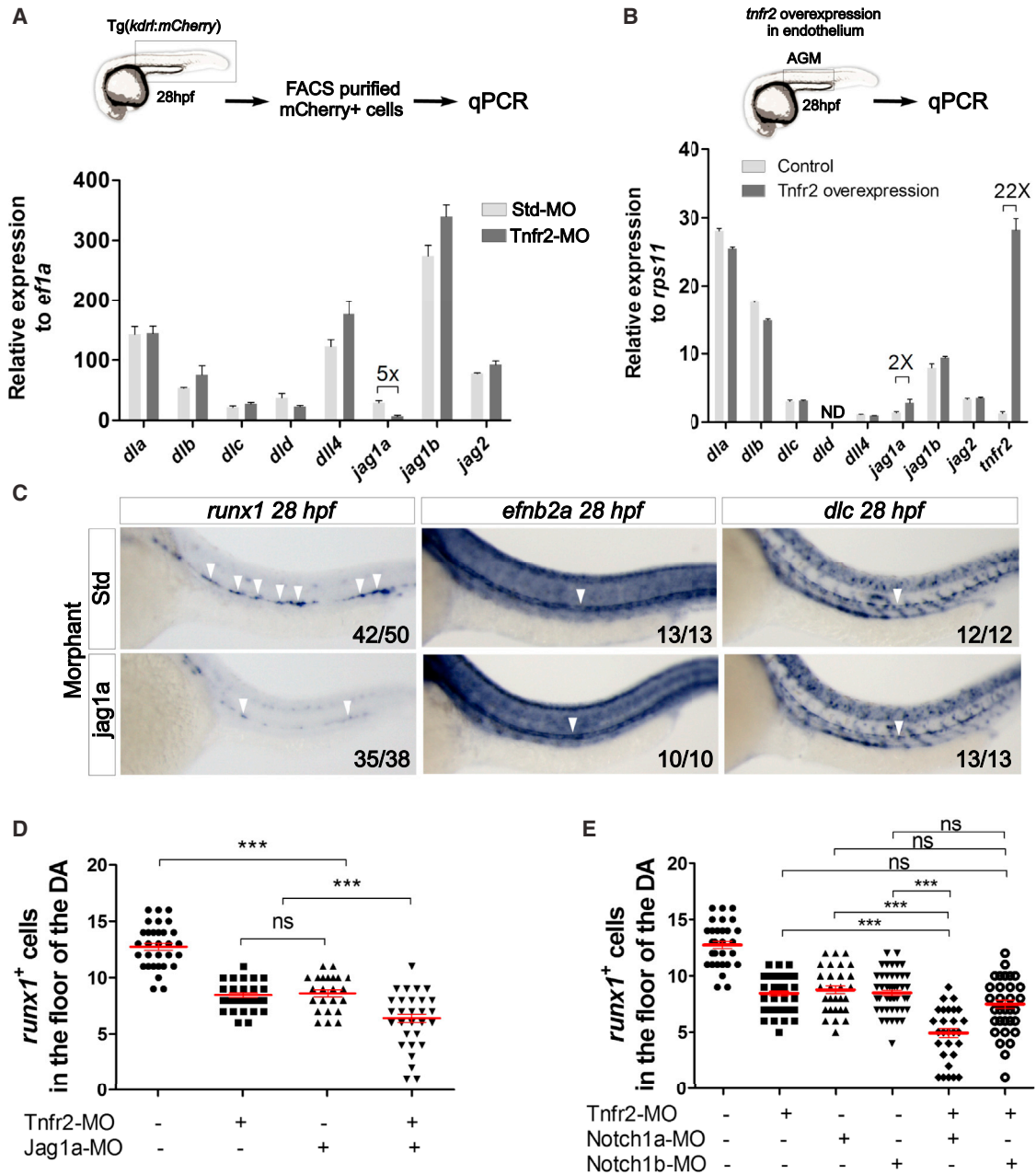


Figure 4. Tnfr2 Induces *jagged1a* in Endothelial Cells, Encouraging HSC Specification

(A) *kdr1:mCherry*⁺ cells from dissected trunks of Std or Tnfr2 morphants were purified by FACS at 28 hpf for qPCR. Levels of indicated transcripts along x axis are shown relative to the housekeeping gene *ef1a*. Bars represent means ± SEM of duplicate samples.

(B) AGM regions from *fli1a:Gal4*; *UAS:tnfr2* embryos were dissected and subjected to qPCR for transcripts shown along x axis. Bars represent means ± SEM of triplicate samples expression relative to the housekeeping gene *rps11*.

(C) Std (top) or *Jag1a* (bottom) morphants were interrogated for *runx1* expression at 26 hpf and *efnb2a* and *dlc* at 28 hpf by WISH. Numbers represent larvae with indicated phenotype.

(D) Enumeration of *runx1*⁺ cells in Tnfr2 and/or *Jag1a* morphants at 28 hpf.

(E) Enumeration of *runx1*⁺ cells in Tnfr2 and/or Notch1a and/or Notch1b morphants at 28 hpf. Each dot is the number of HSCs per embryo, and red lines indicate means ± SEM (D and E) ***p < 0.001; ns, not significant.

See also Figure S3.

findings demonstrate that production of Tnfa from primitive neutrophils is critical for the specification and/or maintenance of HSC fate.

Overall, these data indicate that production of Tnfa from primitive neutrophils activates Tnfr2, upregulating the expression of *Jag1a* on the surface of endothelial cells. *Jag1a* in turn activates

Notch1a, triggering a signaling cascade whereby NF- κ B triggers a transcriptional program required for the emergence of HSCs from hemogenic endothelium (Figures S5C and S5D).

DISCUSSION

Traditionally, infection and inflammation were thought to play an indirect role in HSC homeostasis by causing increased proliferation and skewed differentiation toward microbicidal immune cell lineages (Takizawa et al., 2012). However, recent studies indicate that HSCs can respond directly to the inflammatory cytokines interferon (IFN) α/β , γ , and TNF α (Baldrige et al., 2011; King and Goodell, 2011). Additionally, there is evidence that HSCs can upregulate cytokines under stress-induced hematopoiesis (Zhao et al., 2014). Here, we examined a much earlier step in the biology of HSCs—their specification and emergence from hemogenic endothelium in the developing embryo. The emergence of HSCs from the aortic floor is transient and occurs during developmental windows when the surrounding environment is relatively sterile, whether it is in utero in mammals or within the chorion in teleosts. It is therefore surprising that a key pathway underlying the canonical response to infection and inflammation is required to generate the founders of the adult hematopoietic system. Our studies in the zebrafish demonstrate that depletion of Tnfa or its cognate receptor Tnfr2 leads to depletion of emerging HSCs. The key event elaborated by Tnfr2 appears to be activation of the Notch pathway because ectopic provision of Notch signaling rescued HSCs in the absence of Tnfa or Tnfr2 function. Although Notch signaling is required for HSC specification across vertebrate phyla, little is known regarding how this Notch event is regulated or which of the many receptors or ligands are necessary to fate HSCs from ventral aortic endothelium.

That the HSC program can be rescued in either Tnfa or Tnfr2 morphants by enforced expression of NICD1a within the vasculature demonstrates that the TNF pathway lies upstream of Notch in HSC specification. Our results suggest that signaling via Tnfr2 specifically controls Notch activation by inducing the Notch ligand *jag1a* in cells within the DA. Synergy experiments depleting Notch1a and Tnfr2 combinatorially indicate that Notch1a is likely the receptor on HSCs that binds to the Jag1a ligand presented by aortic endothelial cells. These findings are consistent with studies in the mouse embryo, where Notch1 is required cell autonomously within HSCs or their lineal precursors for their specification (Hadland et al., 2004; Kumano et al., 2003). The zebrafish Notch1a and Notch1b receptors are evolutionary paralogues of mammalian Notch1 (Kortschak et al., 2001) and are both expressed in the DA during the window of HSC emergence (Quillien et al., 2014). Our findings extend these results by demonstrating that Notch1 function is evolutionarily conserved in the specification of HSCs and provide a more detailed mechanism regarding how Notch1 may actually function in this process. Further studies will be required to determine the precise interactions between Jag1a and Notch1a and how these interactions lead to establishment of HSC fate.

In addition to its regulation of the Notch pathway, our results also suggest that Tnfa exerts its effects through NF- κ B. Although NF- κ B is known to play a key role in adult mammalian hematopoi-

esis (Gerondakis et al., 2012), a role in the embryonic emergence of HSCs has not been reported. The utilization of a NF- κ B:GFP reporter line allowed us to image the in vivo activation of NF- κ B, indicating that this activation is required within endothelial cells of the DA for HSC emergence. Furthermore, these studies suggest that this activity is downstream of Tnfa/Tnfr2 signaling. Intriguingly, these data also demonstrate that NF- κ B⁺ cells in the floor of the DA are often positive for Notch activity when assessed along with the *tp1* Notch reporter line. Whereas recent evidence suggests that Notch1 can modulate NF- κ B activity in different cellular contexts, it remains to be determined whether one factor is epistatic to the other or if both may operate together within the hemogenic endothelium to establish HSC fate.

In this study, we have also discovered an unexpected role for neutrophils in HSC development. Whereas macrophages are involved in a broad array of developmental processes (Wynn et al., 2013), an active role for neutrophils in modulating developmental events has not been described. Here, we report for the first time that primitive neutrophils are a major source of Tnfa and that the loss of either neutrophils or Tnfa results in the loss of developing HSCs. The prevailing view that primitive myeloid cells have evolved predominantly to provide early immunity is thus likely oversimplistic. At any time point during HSC emergence, whether early during HSC specification or later during EHT, we observed \sim 2-fold decreases in HSC number. That the lineal descendants of HSCs, most importantly T lymphocytes, are absent by 4–5 dpf indicates that the Tnfa/Tnfr2 signaling axis is required to sustain HSC function. Collectively, our findings suggest that activation of Tnfr2 is important both in hemogenic endothelium and in maintaining nascent HSC fate. It is important to note that *tnfa* is also expressed in endothelial cells (data not shown); contribution from the endothelium may thus play a role in either or both of these processes. The means to create conditional, tissue-specific gene disruption in the zebrafish will be required to precisely address the relative importance of each source.

In conclusion, we show that TNF α , a cytokine that has become the paradigm for induction of inflammatory responses, is also key in the establishment of the hematopoietic system through its influence on HSC formation in the developing embryo. In addition to the known signaling inputs required to establish HSC fate, inflammatory signals should now be added to this list. A major challenge for the field is to integrate each of these required inputs to better understand their spatial and temporal requirements, such that this knowledge may be utilized to instruct HSC fate in vitro from human pluripotent precursors, a major unrealized goal of regenerative medicine.

EXPERIMENTAL PROCEDURES

Zebrafish Husbandry and Strains

Zebrafish embryos and adults were mated, staged, raised, and processed as described (Westerfield, 2000) and maintained in accordance with UCSD IACUC guidelines. See Extended Experimental Procedures for description of transgenic lines.

Heat-Shock Treatment

For induction of *hsp70l:Gal4*-driven transgenes, embryos were placed in E3 medium and transferred to a 38°C water bath for 45 min at noted stages.

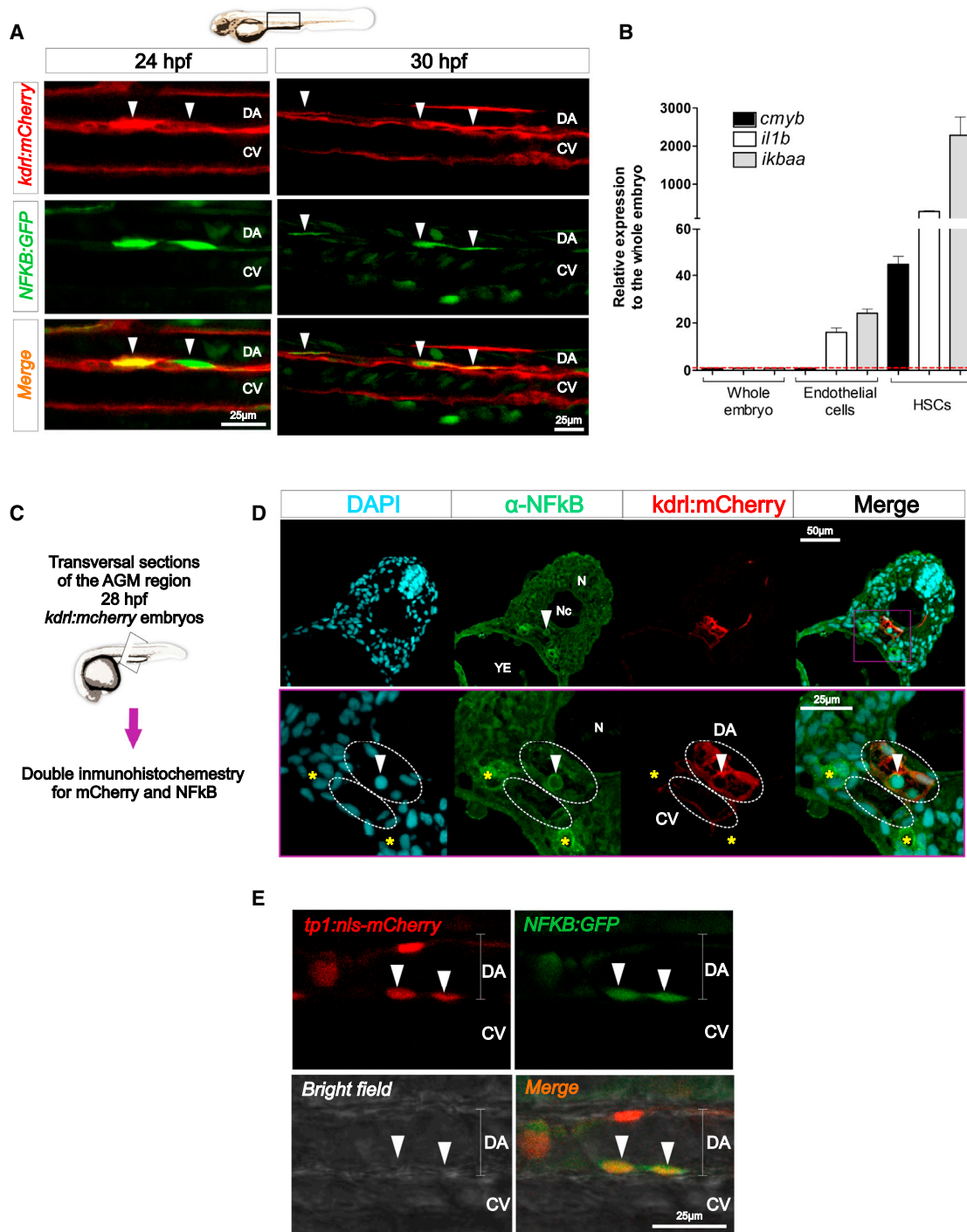


Figure 5. NF-κB Is Active in Emerging HSCs

(A) Trunk region of *kdr1:mCherry*; *NFKB:GFP* double-transgenic animals visualized by confocal microscopy at 24 hpf (left) and 30 hpf (right). Each image is a 2 μ m slice. Arrowheads denote HSCs.

(B) *cmyb*⁻, *kdr1*⁺ endothelial cells and *cmyb*⁺, *kdr1*⁺ HSCs were isolated by FACS at 48 hpf. Levels of the NF-κB target genes *ikbaa* and *il1b*, as well as the HSC marker *cmyb*, are shown relative to *ef1a*. Bars represent means \pm SEM of two biological replicates.

(C) Schematic representation of the experimental design of (D). 28 hpf *kdr1:mCherry* animals were transversally sectioned and subjected to double immunohistochemistry for mCherry (red) and NF-κB (green). DAPI (blue) was added to visualize nuclei.

(legend continued on next page)

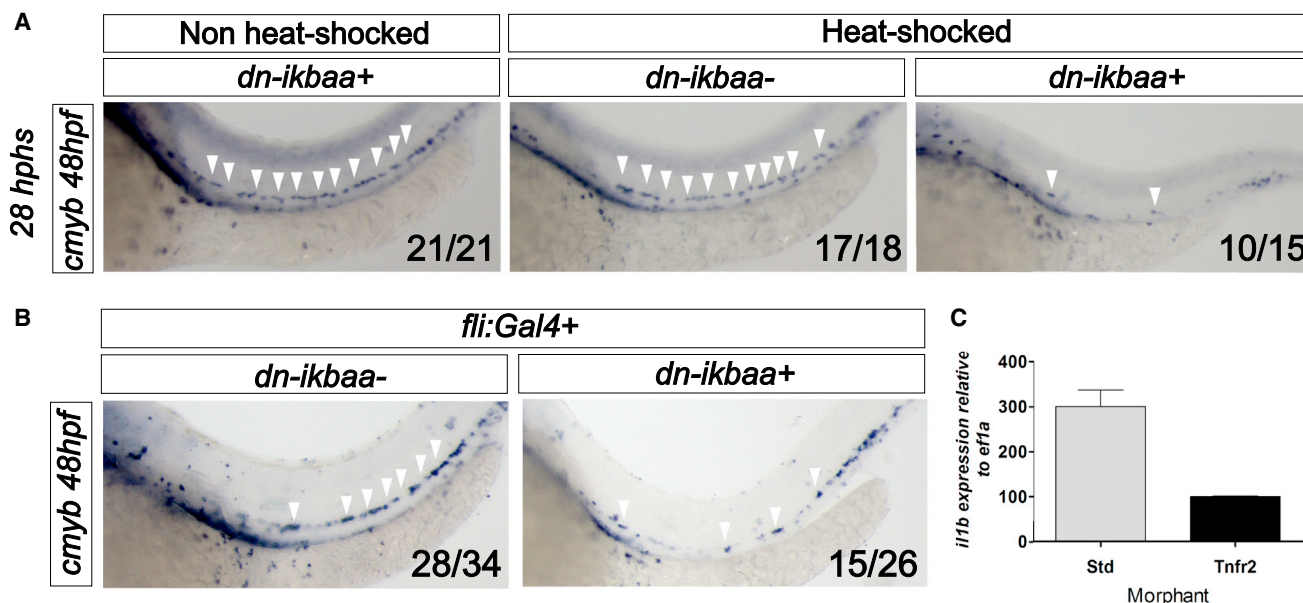


Figure 6. NF- κ B Is Required for HSC Specification and Acts Downstream of Tnfr2

(A) *hsp70:Gal4; UAS:dn-ikbaa* embryos were heat shocked at 20 hpf. WISH for *cmyb* was performed at 48 hpf.

(B) WISH for *cmyb* in *fli1a:Gal4; UAS:dn-ikbaa⁻* (left) and *fli1a:Gal4; UAS:dn-ikbaa⁺* (right) embryos. Arrowheads mark *cmyb⁺* cells along the DA.

(C) *kdr1:mCherry⁺* cells were FACS sorted from Std or Tnfr2 morphants at 28 hpf for qPCR. Levels of the NF- κ B target gene *il1b* are shown relative to *ef1a*. Bars represent means \pm SEM from duplicate samples.

See also Figure S4.

Generation of Transgenic Animals

Tg (UAS:dnnfkb1a)^{sd35} and *Tg (UAS:tnfr2)^{ums1}* embryos were generated by Tol2-mediated transgenesis via the multisite Gateway cloning system (Invitrogen). See also Extended Experimental Procedures.

Morpholino Injection

Specific antisense targeting MOs (Gene Tools) were resuspended in DEPC-treated water at 1–3 mM and injected in one-cell stage embryos. See also Extended Experimental Procedures.

Enumeration of HSCs

Animals were subjected to WISH for *runx1* and *cmyb* at noted stages, and positive cells were imaged and manually counted. Confocal microscopy was performed on *cmyb:GFP; kdr1:mCherry* double-transgenic animals (Bertrand et al., 2010a), *tp1:eGFP; kdr1:mCherry* double-transgenic animals, and *NF- κ B:GFP; kdr1:mCherry* double-transgenic animals. Z sections of the DA region were captured on a Leica SP5 microscope (Leica) using Volocity Acquisition, Visualization, and Restoration software (Improvision) and were manually counted.

Fluorescent Visualization of Blood Flow, HSPCs, and T Cells

To visualize blood flow, HSPCs, and T cells, *cd41:eGFP; gata1:dsred* embryos at 3 dpf and *lck:GFP* larvae at 4 dpf, respectively, were anesthetized in Tricaine (200 μ g/ml) and examined using a Leica MZ16FA stereomicroscope.

Flow Cytometry and FACS

Briefly, embryos were dechorionated with pronase, anesthetized in tricaine, and dissociated with liberase or triturated with a P1000 pipette. The resulting suspension was filtered with a 40 μ m cell strainer, and flow cytometric acqui-

sitions or FACS were performed on a FACS LSRII. See also Extended Experimental Procedures.

Whole-Mount RNA In Situ Hybridization

WISH was carried out as described (Thisse et al., 1993). Probes for the *gata1a*, *csfr1ra*, *kdr1*, *cmyb*, *runx1*, *foxn1*, *efnb2a*, *dlc*, *notch1b*, *notch3*, and *rag1* transcripts were generated using the DIG RNA Labeling Kit (Roche Applied Science) from linearized plasmids. *dn-ikbaa* probe was generated from bp 118–933 of *dn-ikbaa* (see Figure S2). Embryos were imaged using a Leica M165C stereomicroscope equipped with a DFC295 color digital camera (Leica) and FireCam software (Leica).

Statistical Analyses

Data were analyzed by analysis of variance (ANOVA). In all figures, solid red bars denote the mean, and error bars represent SEM. * $p < 0.05$, ** $p < 0.01$, and *** $p < 0.001$; n.s., not significant; n.d., not detected.

Quantitative RT-PCR Analysis

RNA was isolated from tissues with RNeasy (QIAGEN), and cDNA was generated with qScript Supermix (Quanta BioSciences). Primers to detect zebrafish transcripts are described in Table S1. Relative expression levels of genes were calculated by the following formula: relative expression = $2^{-C_t(\text{gene of interest}) - C_t(\text{housekeeping gene})}$.

Immunofluorescence of NICD⁺ Animals

The immunofluorescence staining for cMyc in *hsp70:gal4; UAS:NICD-myc* zebrafish embryos was performed as previously described (Kim et al., 2014).

(D) Maximum projections of 1 μ m sections. Arrowhead indicates a potential HSC emerging in the DA. DA and CV are demarcated by dashed white lines. Yellow asterisks indicate pronephric ducts.

(E) *tp1:nls-mCherry; NFkB:GFP* animals were visualized by confocal microscopy at 24 hpf. Each image is a 2 μ m z slice. Arrowheads indicate HSCs. CV, caudal vein; DA, dorsal aorta; N, neural tube; Nc, notochord; YE, yolk extension.

See also Movie S1.

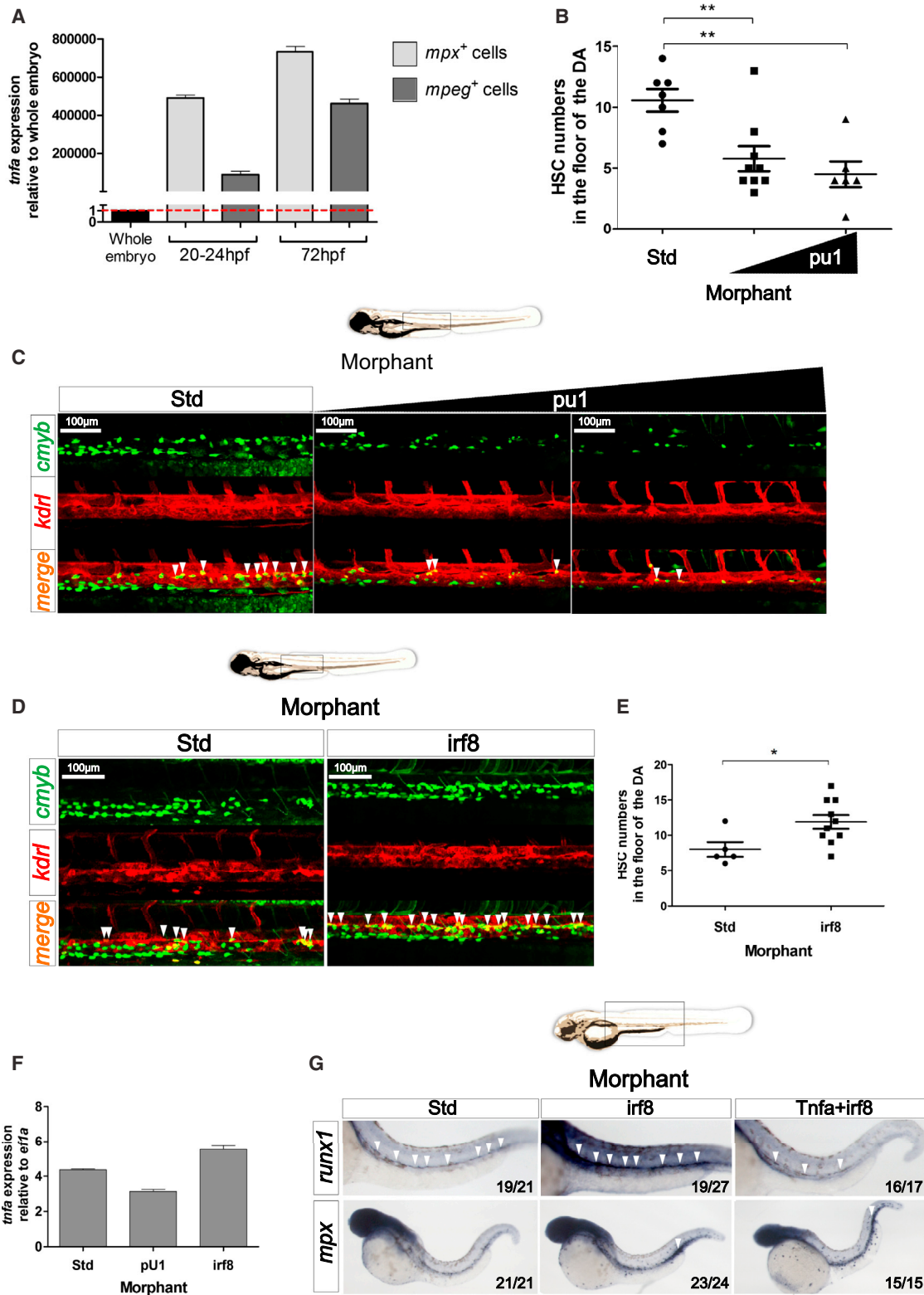


Figure 7. Primitive Myeloid Cells Play a Key Role in HSC Specification

(A) Primitive neutrophils (*mpx*:GFP⁺) and macrophages (*mpeg*:GFP⁺) were isolated at 20–24 and 72 hpf by FACS and *tnfa* expression was quantified by qPCR. Expression was normalized to *ef1a* and is presented relative to whole-embryo expression. Bars represent means ± SEM of two independent experiments.

(legend continued on next page)

Detection of Apoptotic Cell Death by TUNEL Labeling

The TUNEL assay was performed as previously described (Espín et al., 2013) with slight modifications. See also [Extended Experimental Procedures](#).

Lipopolysaccharide Injections

Tg(*hsp:Gal4*; *UAS:dn-ikbaa*) embryos were manually dechorionated at 24 hpf, followed by heat shock at 38°C for 50 min. Four hr post-heat-shock, 2 nl of PBS or LPS (900 µg/ml) (L6511, Sigma) was injected into the posterior blood island (PBI). Embryos were then harvested 1 hr postinjection (hpi), and RNA was isolated for qPCR analysis.

Microtome Sections and Immunohistochemistry

Embryos were fixed with 4% PFA, embedded in paraffin, and sectioned at 5 µm in thickness with Leica microtome. Immunohistochemistry was performed as previously described (Kobayashi et al., 2014). The following antibodies were used: mouse anti-mCherry 1:500 (Abcam, ab125096), rabbit anti-p65 (NF-κB) (RB-1638-P; Lab Vision) 1:200, donkey anti-rabbit IgG Alexa Fluor 594-conjugated (Molecular Probes, A-21207) 1:1,000, and donkey anti-mouse IgG Alexa Fluor 488-conjugated (Molecular Probes, A-11029) in addition to DAPI 1:1000 (Life Technologies, D3571).

SUPPLEMENTAL INFORMATION

Supplemental Information includes Extended Experimental Procedures, five figures, one table, and one movie and can be found with this article online at <http://dx.doi.org/10.1016/j.cell.2014.10.031>.

AUTHOR CONTRIBUTIONS

All studies presented herein derive from initial observations by R.E.-P. in the laboratory of V.M. R.E.-P., D.L.S., C.A.C., N.D.C., A.D.K., J.M., D.T., and V.M. designed experiments; R.E.-P., D.L.S., C.A.C., D.G.-M., N.D.C., and S.C. performed research; R.E.-P., D.L.S., C.A.C., D.G.-M., N.D.C., A.D.K., S.C., J.M., V.M., and D.T. analyzed data; and R.E.-P., D.L.S., V.M., and D.T. wrote the paper with minor contributions from the remaining authors.

ACKNOWLEDGMENTS

This work was supported by the Spanish Ministry of Science and Innovation (grants BIO2011-23400, and CSD2007-00002 to V.M.), the Fundación Séneca, Agencia Regional de Ciencia y Tecnología de la Región de Murcia (grant 04538/GERM/06 to V.M. and predoctoral and postdoctoral fellowships to R.E.-P.), the NIH (K01-DK087814-01A1; D.L.S.), a CIRM New Faculty Award RN1-00575-1 (D.T.), AHA Innovative Science Award 12PILT12860010 (D.T.), and NIH R01-DK074482 (D.T.). We thank Inmaculada Fuentes, Pedro Martínez, Efrén Reyes, Chase Melick, and Karen Ong for technical assistance; Nadia Mercader for ideas and discussion; Francisco Juan Martínez-Navarro and Liangdao Li for help with WISH; and Kylie Price and SAI staff for flow cytometry.

Received: April 11, 2014

Revised: September 17, 2014

Accepted: October 15, 2014

Published: November 6, 2014

REFERENCES

- Abbas, S., and Abu-Amer, Y. (2003). Dominant-negative IkappaB facilitates apoptosis of osteoclasts by tumor necrosis factor-alpha. *J. Biol. Chem.* *278*, 20077–20082.
- Aggarwal, B.B. (2003). Signalling pathways of the TNF superfamily: a double-edged sword. *Nat. Rev. Immunol.* *3*, 745–756.
- Aggarwal, B.B., Gupta, S.C., and Kim, J.H. (2012). Historical perspectives on tumor necrosis factor and its superfamily: 25 years later, a golden journey. *Blood* *119*, 651–665.
- Ahn, K.S., and Aggarwal, B.B. (2005). Transcription factor NF-kappaB: a sensor for smoke and stress signals. *Ann. N Y Acad. Sci.* *1056*, 218–233.
- Ang, H.L., and Tergaonkar, V. (2007). Notch and NFkappaB signaling pathways: Do they collaborate in normal vertebrate brain development and function? *Bioessays* *29*, 1039–1047.
- Baldrige, M.T., King, K.Y., and Goodell, M.A. (2011). Inflammatory signals regulate hematopoietic stem cells. *Trends Immunol.* *32*, 57–65.
- Bertrand, J.Y., Kim, A.D., Teng, S., and Traver, D. (2008). CD41+ cmyb+ precursors colonize the zebrafish pronephros by a novel migration route to initiate adult hematopoiesis. *Development* *135*, 1853–1862.
- Bertrand, J.Y., Chi, N.C., Santoso, B., Teng, S., Stainier, D.Y., and Traver, D. (2010a). Haematopoietic stem cells derive directly from aortic endothelium during development. *Nature* *464*, 108–111.
- Bertrand, J.Y., Cisson, J.L., Stachura, D.L., and Traver, D. (2010b). Notch signaling distinguishes 2 waves of definitive hematopoiesis in the zebrafish embryo. *Blood* *115*, 2777–2783.
- Bigas, A., and Espinosa, L. (2012). Hematopoietic stem cells: to be or Notch to be. *Blood* *119*, 3226–3235.
- Bigas, A., Robert-Moreno, A., and Espinosa, L. (2010). The Notch pathway in the developing hematopoietic system. *Int. J. Dev. Biol.* *54*, 1175–1188.
- Bigas, A., Guiu, J., and Gama-Norton, L. (2013). Notch and Wnt signaling in the emergence of hematopoietic stem cells. *Blood Cells Mol. Dis.* *51*, 264–270.
- Boisset, J.C., van Cappellen, W., Andrieu-Soler, C., Galjart, N., Dzierzak, E., and Robin, C. (2010). In vivo imaging of haematopoietic cells emerging from the mouse aortic endothelium. *Nature* *464*, 116–120.
- Brown, K.D., Claudio, E., and Siebenlist, U. (2008). The roles of the classical and alternative nuclear factor-kappaB pathways: potential implications for autoimmunity and rheumatoid arthritis. *Arthritis Res. Ther.* *10*, 212.
- Burns, C.E., Traver, D., Mayhall, E., Shepard, J.L., and Zon, L.I. (2005). Hematopoietic stem cell fate is established by the Notch-Runx pathway. *Genes Dev.* *19*, 2331–2342.
- Cao, Q., Kaur, C., Wu, C.Y., Lu, J., and Ling, E.A. (2011). Nuclear factor-kappa β regulates Notch signaling in production of proinflammatory cytokines and nitric oxide in murine BV-2 microglial cells. *Neuroscience* *192*, 140–154.
- Clements, W.K., and Traver, D. (2013). Signalling pathways that control vertebrate haematopoietic stem cell specification. *Nat. Rev. Immunol.* *13*, 336–348.
- Cole, L.K., and Ross, L.S. (2001). Apoptosis in the developing zebrafish embryo. *Dev. Biol.* *240*, 123–142.

(B) Enumeration of *cmyb*⁺; *kdr1*⁺ HSCs shown in (C). Each dot represents total *cmyb*⁺; *kdr1*⁺ cells per embryo, and black lines indicate means ± SEM for each group of embryos. **p<0.01.

(C) Maximum projections of representative images of *cmyb:GFP*; *kdr1:mCherry* embryos at 48 hpf following injections of Std or pu1 MOs, the latter at two different concentrations. Region shown is the DA, and arrowheads denote *cmyb*⁺; *kdr1*⁺ HSCs.

(D) Maximum projections of representative images of *cmyb:GFP*; *kdr1:mCherry* embryos at 48 hpf in Std and *irf8* morphants. Arrowheads denote *cmyb*⁺; *kdr1*⁺ HSCs.

(E) Enumeration of *cmyb*⁺; *kdr1*⁺ HSCs shown in (D).

(F) *tnfa* expression relative to *ef1a* in 28 hpf Std, pu1, or *irf8* morphants. Bars represent means ± SEM of duplicate samples.

(G) Std, *irf8*, and *irf8+Tnfa* morphants were interrogated by WISH for *runx1* and *mpx* at 28 hpf. All views are lateral, with anteriors to the left. Numbers represent larvae with indicated phenotypes. *p < 0.05 and ***p < 0.001.

See also [Figure S5](#).

- de Bruijn, M.F., Speck, N.A., Peeters, M.C., and Dzierzak, E. (2000). Definitive hematopoietic stem cells first develop within the major arterial regions of the mouse embryo. *EMBO J.* *19*, 2465–2474.
- Espín, R., Roca, F.J., Candel, S., Sepulcre, M.P., González-Rosa, J.M., Alcaraz-Pérez, F., Meseguer, J., Cayuela, M.L., Mercader, N., and Mulero, V. (2013). TNF receptors regulate vascular homeostasis in zebrafish through a caspase-8, caspase-2 and P53 apoptotic program that bypasses caspase-3. *Dis. Model. Mech.* *6*, 383–396.
- Espinosa, L., Inglés-Esteve, J., Robert-Moreno, A., and Bigas, A. (2003). Ikap-paBalpha and p65 regulate the cytoplasmic shuttling of nuclear corepressors: cross-talk between Notch and NFkappaB pathways. *Mol. Biol. Cell* *14*, 491–502.
- Espinosa, L., Cathelin, S., D'Altri, T., Trimarchi, T., Statnikov, A., Guiu, J., Rodilla, V., Inglés-Esteve, J., Nomdedeu, J., Bellosillo, B., et al. (2010). The Notch/Hes1 pathway sustains NF- κ B activation through CYLD repression in T cell leukemia. *Cancer Cell* *18*, 268–281.
- Faustman, D., and Davis, M. (2010). TNF receptor 2 pathway: drug target for autoimmune diseases. *Nat. Rev. Drug Discov.* *9*, 482–493.
- Fernandez, L., Rodriguez, S., Huang, H., Chora, A., Fernandes, J., Mumaw, C., Cruz, E., Pollok, K., Cristina, F., Price, J.E., et al. (2008). Tumor necrosis factor- α and endothelial cells modulate Notch signaling in the bone marrow microenvironment during inflammation. *Exp. Hematol.* *36*, 545–558.
- Gering, M., and Patient, R. (2005). Hedgehog signaling is required for adult blood stem cell formation in zebrafish embryos. *Dev. Cell* *8*, 389–400.
- Gerondakis, S., Banerjee, A., Grigoriadis, G., Vasanthakumar, A., Gugasyan, R., Sidwell, T., and Grumont, R.J. (2012). NF- κ B subunit specificity in hemopoiesis. *Immunol. Rev.* *246*, 272–285.
- Godin, I., and Cumano, A. (2002). The hare and the tortoise: an embryonic haematopoietic race. *Nat. Rev. Immunol.* *2*, 593–604.
- Hadland, B.K., Huppert, S.S., Kanungo, J., Xue, Y., Jiang, R., Gridley, T., Conlon, R.A., Cheng, A.M., Kopan, R., and Longmore, G.D. (2004). A requirement for Notch1 distinguishes 2 phases of definitive hematopoiesis during development. *Blood* *104*, 3097–3105.
- Herbomel, P., Thisse, B., and Thisse, C. (1999). Ontogeny and behaviour of early macrophages in the zebrafish embryo. *Development* *126*, 3735–3745.
- Herbomel, P., Thisse, B., and Thisse, C. (2001). Zebrafish early macrophages colonize cephalic mesenchyme and developing brain, retina, and epidermis through a M-CSF receptor-dependent invasive process. *Dev. Biol.* *238*, 274–288.
- Johnston, D.A., Dong, B., and Hughes, C.C. (2009). TNF induction of jagged-1 in endothelial cells is NFkappaB-dependent. *Gene* *435*, 36–44.
- Kanther, M., Sun, X., Mühlbauer, M., Mackey, L.C., Flynn, E.J., 3rd, Bagnat, M., Jobin, C., and Rawls, J.F. (2011). Microbial colonization induces dynamic temporal and spatial patterns of NF- κ B activation in the zebrafish digestive tract. *Gastroenterology* *141*, 197–207.
- Kim, A.D., Melick, C.H., Clements, W.K., Stachura, D.L., Distel, M., Panáková, D., MacRae, C., Mork, L.A., Crump, J.G., and Traver, D. (2014). Discrete Notch signaling requirements in the specification of hematopoietic stem cells. *EMBO J.* *33*, 2363–2373.
- King, K.Y., and Goodell, M.A. (2011). Inflammatory modulation of HSCs: viewing the HSC as a foundation for the immune response. *Nat. Rev. Immunol.* *11*, 685–692.
- Kissa, K., and Herbomel, P. (2010). Blood stem cells emerge from aortic endothelium by a novel type of cell transition. *Nature* *464*, 112–115.
- Kobayashi, I., Kobayashi-Sun, J., Kim, A.D., Pouget, C., Fujita, N., Suda, T., and Traver, D. (2014). Jam1a-Jam2a interactions regulate haematopoietic stem cell fate through Notch signalling. *Nature* *512*, 319–323.
- Kohchi, C., Noguchi, K., Tanabe, Y., Mizuno, D., and Soma, G. (1994). Constitutive expression of TNF- α and - β genes in mouse embryo: roles of cytokines as regulator and effector on development. *Int. J. Biochem.* *26*, 111–119.
- Kondo, M., Wagers, A.J., Manz, M.G., Prohaska, S.S., Scherer, D.C., Beilhack, G.F., Shizuru, J.A., and Weissman, I.L. (2003). Biology of hematopoietic stem cells and progenitors: implications for clinical application. *Annu. Rev. Immunol.* *21*, 759–806.
- Kopan, R., and Ilgan, M.X. (2009). The canonical Notch signaling pathway: unfolding the activation mechanism. *Cell* *137*, 216–233.
- Kortschak, R.D., Tamme, R., and Lardelli, M. (2001). Evolutionary analysis of vertebrate Notch genes. *Dev. Genes Evol.* *211*, 350–354.
- Kumano, K., Chiba, S., Kunisato, A., Sata, M., Saito, T., Nakagami-Yamaguchi, E., Yamaguchi, T., Masuda, S., Shimizu, K., Takahashi, T., et al. (2003). Notch1 but not Notch2 is essential for generating hematopoietic stem cells from endothelial cells. *Immunity* *18*, 699–711.
- Kyba, M., and Daley, G.Q. (2003). Hematopoiesis from embryonic stem cells: lessons from and for ontogeny. *Exp. Hematol.* *31*, 994–1006.
- Lai, E.C. (2004). Notch signaling: control of cell communication and cell fate. *Development* *131*, 965–973.
- Langenau, D.M., Ferrando, A.A., Traver, D., Kutok, J.L., Hezel, J.P., Kanki, J.P., Zon, L.I., Look, A.T., and Trede, N.S. (2004). In vivo tracking of T cell development, ablation, and engraftment in transgenic zebrafish. *Proc. Natl. Acad. Sci. USA* *101*, 7369–7374.
- Lawson, N.D., Scheer, N., Pham, V.N., Kim, C.H., Chitnis, A.B., Campos-Ortega, J.A., and Weinstein, B.M. (2001). Notch signaling is required for arterial-venous differentiation during embryonic vascular development. *Development* *128*, 3675–3683.
- Le Guyader, D., Redd, M.J., Colucci-Guyon, E., Murayama, E., Kissa, K., Briolat, V., Mordelet, E., Zapata, A., Shinomiya, H., and Herbomel, P. (2008). Origins and unconventional behavior of neutrophils in developing zebrafish. *Blood* *111*, 132–141.
- Li, L., Jin, H., Xu, J., Shi, Y., and Wen, Z. (2011). Irf8 regulates macrophage versus neutrophil fate during zebrafish primitive myelopoiesis. *Blood* *117*, 1359–1369.
- Mizrahi, K., and Askenasy, N. (2014). Physiological functions of TNF family receptor/ligand interactions in hematopoiesis and transplantation. *Blood* *124*, 176–183.
- Parsons, M.J., Pisharath, H., Yusuff, S., Moore, J.C., Siekmann, A.F., Lawson, N., and Leach, S.D. (2009). Notch-responsive cells initiate the secondary transition in larval zebrafish pancreas. *Mech. Dev.* *126*, 898–912.
- Quillien, A., Moore, J.C., Shin, M., Siekmann, A.F., Smith, T., Pan, L., Moens, C.B., Parsons, M.J., and Lawson, N.D. (2014). Distinct Notch signaling outputs pattern the developing arterial system. *Development* *141*, 1544–1552.
- Rhodes, J., Hagen, A., Hsu, K., Deng, M., Liu, T.X., Look, A.T., and Kanki, J.P. (2005). Interplay of pu.1 and gata1 determines myelo-erythroid progenitor cell fate in zebrafish. *Dev. Cell* *8*, 97–108.
- Robert-Moreno, A., Guiu, J., Ruiz-Herguido, C., López, M.E., Inglés-Esteve, J., Riera, L., Tipping, A., Enver, T., Dzierzak, E., Gridley, T., et al. (2008). Impaired embryonic haematopoiesis yet normal arterial development in the absence of the Notch ligand Jagged1. *EMBO J.* *27*, 1886–1895.
- Roca, F.J., Mulero, I., López-Muñoz, A., Sepulcre, M.P., Renshaw, S.A., Meseguer, J., and Mulero, V. (2008). Evolution of the inflammatory response in vertebrates: fish TNF- α is a powerful activator of endothelial cells but hardly activates phagocytes. *J. Immunol.* *181*, 5071–5081.
- Sainson, R.C., Johnston, D.A., Chu, H.C., Holderfield, M.T., Nakatsu, M.N., Crampton, S.P., Davis, J., Conn, E., and Hughes, C.C. (2008). TNF primes endothelial cells for angiogenic sprouting by inducing a tip cell phenotype. *Blood* *111*, 4997–5007.
- Santoro, M.M., Samuel, T., Mitchell, T., Reed, J.C., and Stainier, D.Y. (2007). Birc2 (clap1) regulates endothelial cell integrity and blood vessel homeostasis. *Nat. Genet.* *39*, 1397–1402.
- Shalaby, M.R., Sundan, A., Loetscher, H., Brockhaus, M., Lesslauer, W., and Espevik, T. (1990). Binding and regulation of cellular functions by monoclonal antibodies against human tumor necrosis factor receptors. *J. Exp. Med.* *172*, 1517–1520.
- Shin, H.M., Minter, L.M., Cho, O.H., Gottipati, S., Fauq, A.H., Golde, T.E., Sonnenshein, G.E., and Osborne, B.A. (2006). Notch1 augments NF- κ B activity by facilitating its nuclear retention. *EMBO J.* *25*, 129–138.

- Song, L.L., Peng, Y., Yun, J., Rizzo, P., Chaturvedi, V., Weijzen, S., Kast, W.M., Stone, P.J., Santos, L., Loreda, A., et al. (2008). Notch-1 associates with IKK α and regulates IKK activity in cervical cancer cells. *Oncogene* 27, 5833–5844.
- Stein, S.J., and Baldwin, A.S. (2013). Deletion of the NF- κ B subunit p65/RelA in the hematopoietic compartment leads to defects in hematopoietic stem cell function. *Blood* 121, 5015–5024.
- Takizawa, H., Boettcher, S., and Manz, M.G. (2012). Demand-adapted regulation of early hematopoiesis in infection and inflammation. *Blood* 119, 2991–3002.
- Thisse, C., Thisse, B., Schilling, T.F., and Postlethwait, J.H. (1993). Structure of the zebrafish *snail1* gene and its expression in wild-type, spadetail and no tail mutant embryos. *Development* 119, 1203–1215.
- van der Vaart, M., van Soest, J.J., Spaik, H.P., and Meijer, A.H. (2013). Functional analysis of a zebrafish *myd88* mutant identifies key transcriptional components of the innate immune system. *Dis. Model. Mech.* 6, 841–854.
- Wang, H., Tian, Y., Wang, J., Phillips, K.L., Binch, A.L., Dunn, S., Cross, A., Chiverton, N., Zheng, Z., Shapiro, I.M., et al. (2013). Inflammatory cytokines induce NOTCH signaling in nucleus pulposus cells: implications in intervertebral disc degeneration. *J. Biol. Chem.* 288, 16761–16774.
- Westerfield, M. (2000). *The Zebrafish Book. A guide for the laboratory use of zebrafish (Danio rerio)*, Fourth Edition (Eugene: Univ. of Oregon Press).
- Wiens, G.D., and Glenney, G.W. (2011). Origin and evolution of TNF and TNF receptor superfamilies. *Dev. Comp. Immunol.* 35, 1324–1335.
- Wynn, T.A., Chawla, A., and Pollard, J.W. (2013). Macrophage biology in development, homeostasis and disease. *Nature* 496, 445–455.
- Zhao, C., Xiu, Y., Ashton, J., Xing, L., Morita, Y., Jordan, C.T., and Boyce, B.F. (2012). Noncanonical NF- κ B signaling regulates hematopoietic stem cell self-renewal and microenvironment interactions. *Stem Cells* 30, 709–718.
- Zhao, J.L., Ma, C., O'Connell, R.M., Mehta, A., DiLoreto, R., Heath, J.R., and Baltimore, D. (2014). Conversion of danger signals into cytokine signals by hematopoietic stem and progenitor cells for regulation of stress-induced hematopoiesis. *Cell Stem Cell* 14, 445–459.

RESEARCH ARTICLE

TNF α Impairs Rhabdoviral Clearance by Inhibiting the Host Autophagic Antiviral Response

Raquel Espín-Palazón^{1☉[‡]✉}, Alicia Martínez-López^{2☉}, Francisco J. Roca^{1[‡]✉}, Azucena López-Muñoz¹, Sylwia D. Tyrkalska¹, Sergio Candel¹, Diana García-Moreno¹, Alberto Falco², José Meseguer¹, Amparo Estepa^{2[†]‡}, Victoriano Mulero^{1[†]*}

1 Departamento de Biología Celular e Histología. Facultad de Biología. Universidad de Murcia, IMIB-Arrixaca, Murcia, Spain, **2** Instituto de Biología Celular y Molecular, Universidad Miguel Hernández, Elche, Spain

† Deceased.

☉ These authors contributed equally to this work.

✉ Current address: Department of Cellular and Molecular Medicine, University of California at San Diego, La Jolla, California, United States of America

✉ Current address: Department of Medicine, MRC-Laboratory of Molecular Biology, University of Cambridge, Cambridge, United Kingdom

‡ These two authors have cosupervised this study.

* vmulero@um.es



OPEN ACCESS

Citation: Espín-Palazón R, Martínez-López A, Roca FJ, López-Muñoz A, Tyrkalska SD, Candel S, et al. (2016) TNF α Impairs Rhabdoviral Clearance by Inhibiting the Host Autophagic Antiviral Response. *PLoS Pathog* 12(6): e1005699. doi:10.1371/journal.ppat.1005699

Editor: Sara Cherry, University of Pennsylvania School of Medicine, UNITED STATES

Received: May 18, 2015

Accepted: May 20, 2016

Published: June 28, 2016

Copyright: © 2016 Espín-Palazón et al. This is an open access article distributed under the terms of the [Creative Commons Attribution License](https://creativecommons.org/licenses/by/4.0/), which permits unrestricted use, distribution, and reproduction in any medium, provided the original author and source are credited.

Data Availability Statement: All relevant data are within the paper and its Supporting Information files.

Funding: This study was funded by: MINECO BIO2011-23400 (VM), MINECO CSD2007-00002 (VM), MINECO BIO2014-52655-R (VM), MINECO AGL2014-51773-C3-1-R (AE), and Fondos Europeos de Desarrollo Regional (FEDER) (VM AE). The funders had no role in study design, data collection and analysis, decision to publish, or preparation of the manuscript.

Abstract

TNF α is a pleiotropic pro-inflammatory cytokine with a key role in the activation of the immune system to fight viral infections. Despite its antiviral role, a few viruses might utilize the host produced TNF α to their benefit. Some recent reports have shown that anti-TNF α therapies could be utilized to treat certain viral infections. However, the underlying mechanisms by which TNF α can favor virus replication have not been identified. Here, a rhabdoviral infection model in zebrafish allowed us to identify the mechanism of action by which Tnfa has a deleterious role for the host to combat certain viral infections. Our results demonstrate that Tnfa signals through its receptor Tnfr2 to enhance viral replication. Mechanistically, Tnfa does not affect viral adhesion and delivery from endosomes to the cytosol. In addition, the host interferon response was also unaffected by Tnfa levels. However, Tnfa blocks the host autophagic response, which is required for viral clearance. This mechanism of action provides new therapeutic targets for the treatment of SVCV-infected fish, and advances our understanding of the previously enigmatic deleterious role of TNF α in certain viral infections.

Author Summary

Tumor necrosis factor alpha (TNF α) is one of the main pro-inflammatory cytokines produced in response to a broad type of infections [1]. Although TNF α has a crucial role in protecting the host organism from pathogens, its deregulation can promote susceptibility

Competing Interests: The authors have declared that no competing interests exist.

to pathogens by impairing pathogen clearance and, ultimately, promoting maintenance of infection and death. In addition, some viruses might utilize the host produced TNF α to their benefit. Thus, anti-TNF α therapies could be utilized to treat certain viral infections. However, the underlying mechanisms by which TNF α can favor certain virus replication have not been identified. Here, we have used a viral infection model in zebrafish to identify the mechanism of action by which TNF α has a deleterious role for the host to combat certain viral infections. Our results demonstrate that *Tnfa* does not affect viral ability to infect host cells or to antagonize the main host antiviral pathway, namely the interferon pathway. However, *Tnfa* impairs viral clearance by blocking the host autophagy response, which is usually used by host cells to degrade unnecessary or dysfunctional cellular components, and that we found to be critical to eliminate intracellular viral particles. This mechanism of action provides new therapeutic targets for the treatment of SVCV-infected fish in aquaculture and probably to other viral infection affecting cattle industry and human.

Introduction

Tumor necrosis factor alpha (TNF α) is one of the main pro-inflammatory cytokines produced in response to a broad type of bacterial, viral and fungal infections [1]. TNF α has a crucial role in activating and orchestrating the immune response in order to protect the host organism from pathogens. TNF α deregulation can promote susceptibility to pathogens by impairing pathogen clearance and, ultimately, promoting maintenance of infection and death. When specifically talking about viral pathogenesis, TNF α has been shown to inhibit the replication of certain viruses such as hepatitis B virus (HBV) and the varicella zoster virus (VZV) [2]. In addition, anti-TNF therapies to treat autoimmune diseases exacerbate the infection produced by virus such as herpes simplex virus (HSV), Epstein-Barr virus (EBV), cytomegalovirus (CMV) and human papillomavirus (HPV) [3]. It is not surprising that due to the key role of TNF α in the host protection to viral infections, some viruses have developed different ways to interfere with the TNF α pathway [4]. In contrast, it seems that a few viruses might utilize the host produced TNF α to their benefit. Interestingly, human immunodeficiency virus 1 (HIV-1) infection induces TNF α expression. These increased TNF α levels in serum correlates to increased viral replication [5]. In accordance to that, TNF α inhibitors are able to impair HIV-1 replication [6], and anti-TNF α treatments have been proposed to combat HIV-1 infection in combination with other therapies [7] [5]. Similarly, neutralization of TNF α decreases virus production in CMV-infected macrophages [8]. The ability of TNF α to favor virus replication has also been demonstrated for non-mammalian viruses, such as the spring viremia of carp virus [9], a fish rhabdovirus infecting cyprinids [10,11]. Moreover, intraperitoneally SVCV-infected adult fish, in which recombinant TNF α was administrated simultaneously, has shown a higher mortality rate than fish injected with the virus alone. The mechanism explaining how TNF α facilitates viral infection and its deleterious effects in the host has not yet been proposed.

Since zebrafish is a cyprinid susceptible to SVCV infection, and TNF α can exacerbate SVCV infection, we chose this amenable infection model to investigate how a virus might utilize host produced TNF α to their benefit. To that end, we analyzed the role of zebrafish TNF α (*Tnfa*) in i) the key steps of SVCV pathogenesis: virus adhesion, fusion, and replication; and ii) in the antiviral host response, such as interferon production and autophagy. The results showed that *Tnfa* signaling through its receptor *Tnfr2* inhibits autophagy, leading to impaired viral clearance in SVCV-infected cells. This mechanism of action provides new therapeutic

targets for the treatment of SVCV-infected fish, and advances our understanding of the previously enigmatic deleterious role of TNF α in certain viral infections.

Results

Tnfa increases susceptibility of zebrafish to SVCV infection

As in most infections, Tnfa is up-regulated in response to SVCV infection [12]. Unexpectedly, this up-regulation rather than help to control the infection, has a deleterious role in adult zebrafish [9]. To further study this phenomena, we first investigated whether or not Tnfa was also able to enhance SVCV replication both *in vivo* and *in vitro*. For that, we pre-incubated the zebrafish embryonic fibroblast cell line, ZF4, which expresses both Tnfrs [9], with zebrafish recombinant Tnfa or interferon 1 (Ifn1, also known as Ifnphi1) for 4 hours and, subsequently, the treated cells were infected with SVCV. At 24 hours post-infection (hpi), viral replication, measured as the presence of transcript of the nucleoprotein that forms the SVCV capsid (N protein), was evaluated by RT-qPCR (Fig 1A). N protein transcripts significantly increased in Tnfa-treated cells and significantly decreased in Ifn1-treated cells (Fig 1B), suggesting that Tnfa enhances and Ifn1 decreases viral replication *in vitro*.

Both insufficient and excess Tnfa have been shown to promote susceptibility to mycobacterial infection [13]. We then asked whether endogenous rather than exogenous Tnfa was beneficial or detrimental to the host during SVCV infection. The percentage of animals that survived at 7 days post-infection (dpi) was significantly higher in Tnfa-depleted larvae when compared to controls (Tnfa expressing larvae) (55% versus 30%, respectively) (Fig 1C and 1D and S1A and S1B Fig). The survival percentage of control and Tnfa-depleted uninfected larvae was 100% in both cases. In accordance to these results, qPCR analysis of embryos harvested at 48hpi showed that the highest levels of viral replication (measured as the amount of SVCV N protein mRNA in infected animal tissues) (Fig 1E), and virus particles (measured as the amount of negative sense RNA encoding SVCV G glycoprotein in infected animal tissues) (Fig 1F), were found in control larvae. These results were further confirmed in larva forced to express Tnfa RNA, which showed drastic increased susceptibility to SVCV (Fig 1G and S1C and S1E Fig). Together, these results indicate that Tnfa enhances SVCV replication and pathogenesis *in vivo*.

The Tnfa/Tnfr2 axis mediates increased SVCV replication in zebrafish

TNF α exerts its activity through the binding and activation of two receptors, TNFR1 and TNFR2 (Tumor necrosis factor receptor 1 and 2, respectively) [14]. Tnf receptors are expressed early during zebrafish development [15], and they both have important roles for the clearance of viral infections [16]. To further dissect the contribution of Tnfa signaling in SVCV pathogenesis, we performed loss-of-function experiments for both Tnfa receptors using specific anti-sense morpholinos (MOs) [15] in SVCV-infected embryos (Fig 2A and S1F–S1I Fig). Tnfr2-depleted larvae were distinctly more resistant to SVCV infection compared to their control siblings (60% versus 30%, respectively) (Fig 2B), while Tnfr1-depleted larvae showed a slightly, but statistically significant, reduced survival compare to their control siblings (Fig 2B). This result was supported by increased, or decreased, SVCV replication in Tnfr1- and Tnfr2-depleted larvae, respectively (Fig 2C). Accordingly, the presence of viral genomes was also higher in Tnfr1-depleted larvae and lower in Tnfr2-depleted larvae at 48 hpi (Fig 2D). In addition, larva forced to express a RNA encoding a dominant negative (DN) form of Tnfr2, which is lacking the entire intracellular signaling domain and extinguishes Tnfr2 signaling by trimerization with endogenous Tnfr2 [15], showed increased resistance to SVCV (Fig 2E and

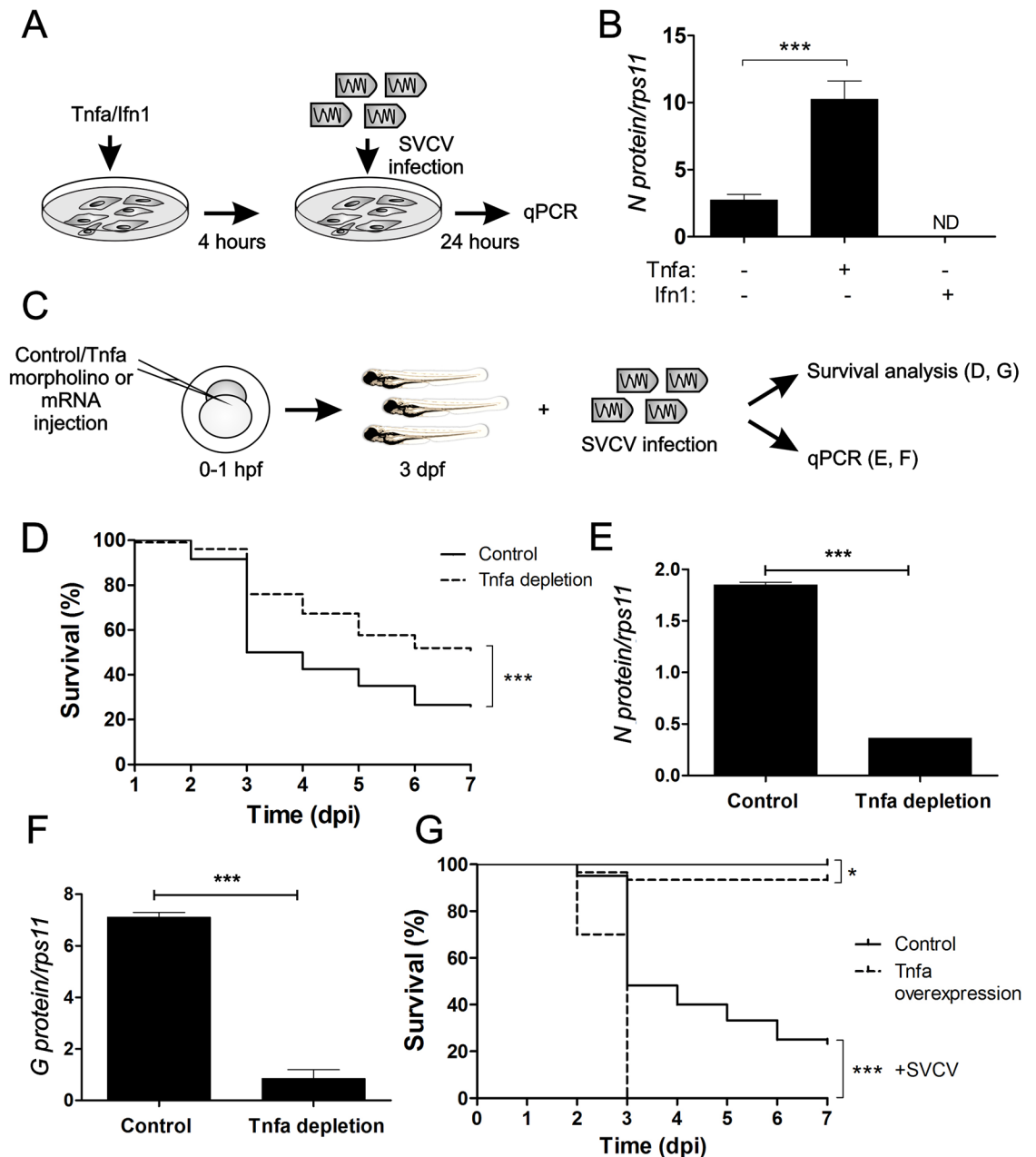


Fig 1. Tnfa enhances SVCV infection in zebrafish. (A) Workflow of the experimental design followed in (B). Recombinant zebrafish Tnfa or interferon 1 (Ifn1) were added to ZF4 cells growing in monolayer at 80% confluence and incubated for 4 hours. Subsequently, the medium was washed out and fresh medium containing SVCV was added. After 24 hours of incubation with the virus, the cells were harvested for qPCR analysis. (B) N protein mRNA expression levels assessed by qPCR relative to the housekeeping gene *rps11* and multiplied by 10^5 . Bars represent mean \pm S.E.M. of indicated gene expression from one representative experiment. (C) Workflow of the experimental design followed in (D-G). Std (Control) or Tnfa mos (D-F) or antisense or Tnfa RNAs (G) were injected in zebrafish embryos at one-cell-stage of development. At 3 dpf, these larvae were immerse in RPMI containing inactivated SVCV (control) or intact SVCV for subsequently analysis of survival (D, G) or qPCR analysis at 48 hours post-infection (hpi) (E, F). Percentage of survival of Tnfa-depleted (D) and overexpressing (G) zebrafish larvae exposed to 10^9 TCID₅₀/ml SVCV. (E, F) The mRNA levels of the gene coding for the SVCV N protein as an estimation of the viral replication (E), and the RNA- levels of G protein (F) were determined in the infected larvae by qPCR in 10 pooled larvae at 48 hpi (5 dpf). The gene expression was normalized against *rps11* and multiplied by 10^5 for N protein. Bars represent mean \pm S.E.M. of triplicate readings from pooled larvae and the data are representative of two independent experiments. *** $p < 0.001$. ND, not detected.

doi:10.1371/journal.ppat.1005699.g001

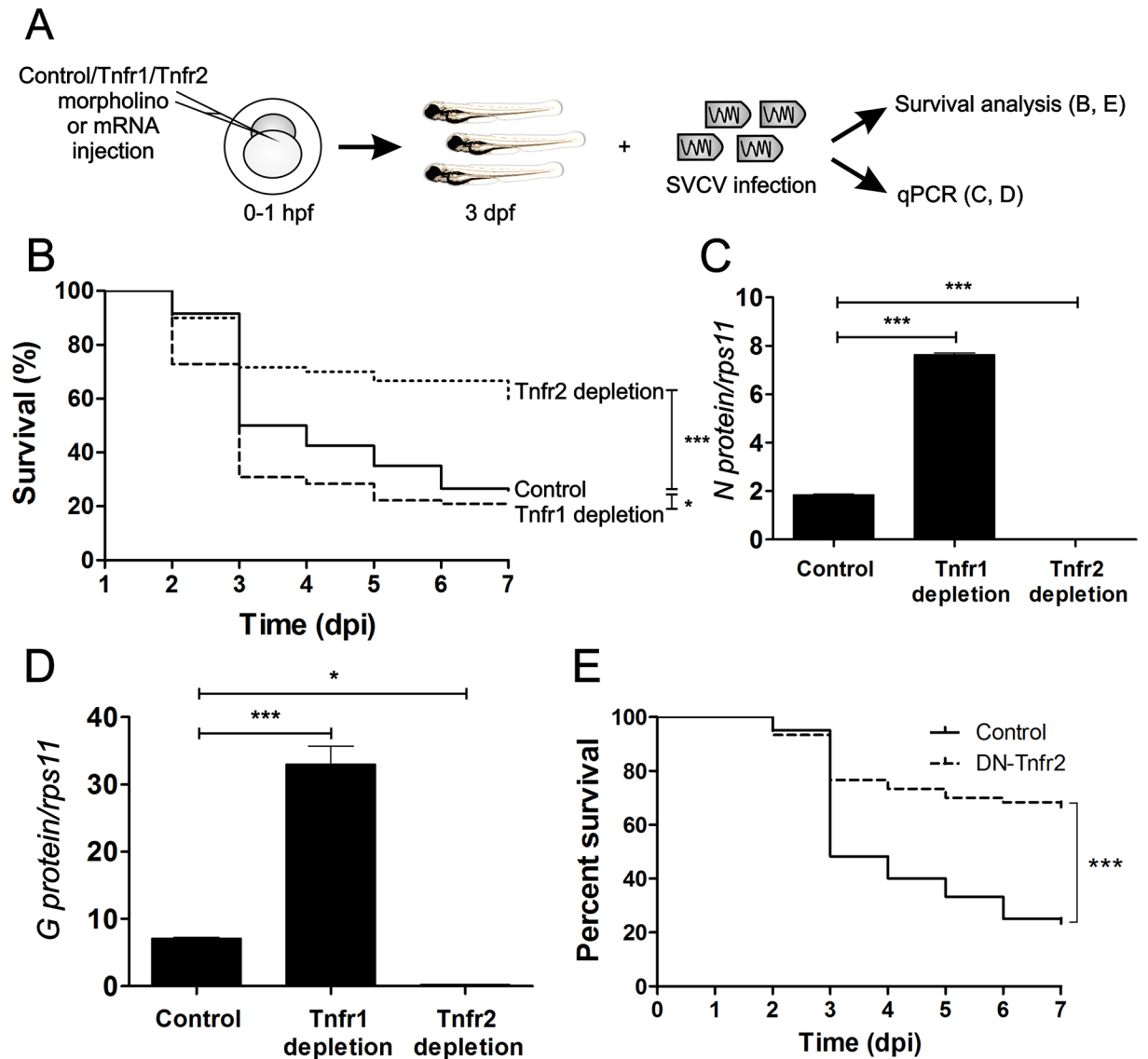


Fig 2. Tnfr2 mediates the Tnfa-triggered susceptibility of zebrafish to SVCV. (A) Workflow of the experimental design followed in (B-E). Std (Control), Tnfr1 or Tnfr2 mos (B-D) or antisense or DN-Tnfr2 RNAs (E) were injected in zebrafish embryos at one-cell-stage of development. At 3 dpf, these larvae were immersed in RPMI containing inactivated SVCV (control) or intact SVCV for subsequent analysis of survival (B, E) or qPCR analysis at 48 hours post-infection (hpi) (C, D). Percentage of survival of Tnfr-depleted (B) and DN-Tnfr2 overexpressing (E) zebrafish larvae exposed to 10^9 TCID₅₀/ml SVCV. (C,D) The mRNA levels of the gene coding for the SVCV N protein as an estimation of the viral replication (C), and the RNA-levels of G protein (D) were determined in the infected larvae by qPCR in 10 pooled larvae at 48 hpi (5 dpf). The gene expression was normalized against *rps11* and multiplied by 10^5 for N protein. Bars represent mean \pm S.E.M. of triplicate readings from pooled larvae and the data are representative of two independent experiments. * $p < 0.1$; *** $p < 0.001$.

doi:10.1371/journal.ppat.1005699.g002

(S1D and S1E Fig). Overall, these results suggest that Tnfa facilitates SVCV replication through Tnfr2 signaling.

Tnfa does not affect viral adhesion or viral delivery from endosomes to the cytosol. To better understand the mechanism by which Tnfa enhances viral replication, we investigated the role of Tnfa in two key steps of SVCV pathogenesis, virus cell binding and the subsequent membrane fusion that allows virus release from the endosome to the cytosol. To interrogate if

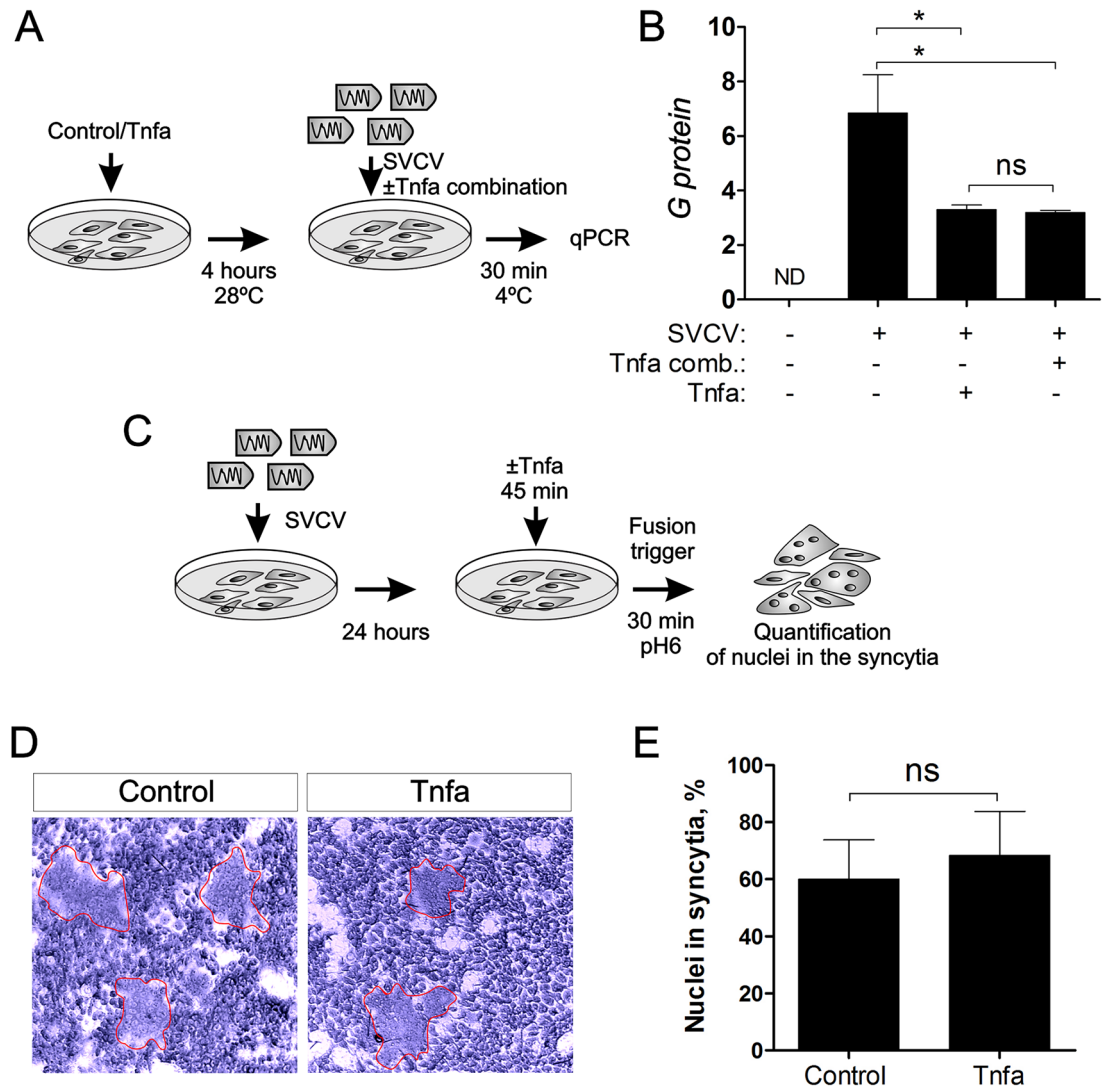


Fig 3. SVCV adhesion or syncytia production is not affected by Tnfa. (A) Workflow of the experimental design followed in (B). Briefly, recombinant zebrafish Tnfa was added to ZF4 cells growing in monolayer at 80% of confluence and incubated for 4 hours. Subsequently, the medium was washed out and new medium containing SVCV ± Tnfa (Tnfa combination) was added for 30 minutes at 4°C to allow virus adhesion but not virus internalization and replication. After 30 minutes, the cells were washed and harvested for qPCR analysis of the G protein gene for quantitation of the adhered virus. (B) qPCR analysis of the G protein encoding gene. Bars represent mean ± S.E.M. of triplicate readings from one sample and the data are representative of two independent experiments. *p<0.1. ns, non significant. Tnfa comb., Tnfa added in combination to the SVCV. (C) Workflow representing the experimental design for (D) and (E). ZF4 were incubated with SVCV for 24 hours. The medium containing virus was washed out and new medium containing Tnfa was added for 45 minutes. The fusion process was triggered by decreasing the pH to 6 for 30 minutes, and the nuclei in the syncytia were quantitated (D, E). Red lines denote syncytia.

doi:10.1371/journal.ppat.1005699.g003

Tnfa could be facilitating the virus binding to the cell, we infected ZF4 cells for 30 minutes at 4°C to allow the virus adhesion but not its endocytosis and replication. Tnfa was added to ZF4 cells before or simultaneously to SVCV (Fig 3A). The number of viral particles adhered to Tnfa-treated cells (in both conditions, pre- or simultaneously added) was slightly lower than in the non-treated cells, assessed by qPCR of negative sense RNA encoding SVCV G glycoprotein (Fig 3B). This result suggests that Tnfa does not facilitate the SVCV cell binding.

After binding to the cell membrane, SVCV enters the cell by receptor-mediated endocytosis. Subsequently, these early endosomes are acidified after fusing to lysosomes. Endosomal acidification triggers conformational changes in the G protein of rhabdovirus, releasing the virus genome into the cytoplasm and allowing their replication [10,17,18]. In order to investigate whether or not this critical step in virus replication was affected by Tnfa, we performed a fusion assay [19] in SVCV-infected ZF4 cells pre-treated with Tnfa, where G-dependent cell fusion is triggered at pH = 6 (Fig 3C). The results show that the fusion process, evaluated by the number of nuclei in syncytia, in Tnfa-treated cells was unaffected compared to non-treated cells (Fig 3D and 3E). Taken together, these data indicate that Tnfa does not facilitate virus binding to the cell membrane or viral genome release into the cytoplasm.

Tnfa does not antagonize the antiviral role of interferon during SVCV infection

Interferon is one of the most powerful antiviral cytokine [20]. It has been shown that interferons can act synergistically with TNF α to suppress virus replication [21,22]. However, TNF α and interferon can have antagonistic roles in certain cells such as human fibroblast-like synovocytes [23]. Therefore, we decided to investigate if the enhancing role of TNF α in SVCV replication was the result of impairing the interferon response during SVCV infection. ZF4 cells were pre-treated with Tnfa and/or Ifn1 for 4 hours. Subsequently, these cells were infected with SVCV alone or in combination with Tnfa. After 24 hours, qPCR analysis was performed to detect the expression of antiviral host genes and viral N protein transcript (Fig 4A). The addition of Tnfa before or in combination with SVCV did not alter the transcript levels of the genes encoding major antiviral effectors, such as myxovirus (influenza) resistance b (Mxb), radical S-adenosyl methionine domain containing 2 (Rsd2), Mxc and protein kinase containing Z-DNA binding domains (Pkz) compared to untreated cells (Fig 4B and 4C and S2A and S2B Fig). In contrast, Ifn1-treated cells showed drastically increased levels of the transcripts for the same host genes (Fig 4B and 4C and S2A and S2B Fig). Cells were then pre-incubated with 2 different dilutions of Ifn1 (1/100 and 1/500), alone or in combination with Tnfa, and subsequent SVCV infection was performed. Both Ifn1 dilutions were able to increase the RNA levels of *mx*b, though these levels were unaffected by the simultaneous addition of Tnfa, in both uninfected and infected cells (Fig 4D). Altogether, these results indicate that Tnfa does not antagonize the antiviral role of Ifn1 during SVCV infection. To verify that Ifn1 was indeed interfering with SVCV replication in ZF4 cells, SVCV replication was quantitated by RT-qPCR analysis of the N protein transcripts in SVCV-infected ZF4 cells pre-treated with Tnfa and Ifn1 (Fig 4A and 4E). While the N protein mRNA levels were up-regulated in Tnfa-treated cells, they were down-regulated in the Ifn1, as well as in the Tnfa/Ifn1 combination (Fig 4E). This finding suggests that Ifn1 has a protective role against SVCV replication and that TNF α does not antagonize the antiviral role of Ifn1 during SVCV infection.

Tnfa inhibits autophagy

Since autophagy is an efficient antiviral mechanism in response to many viral infections including SVCV [24,25], we asked if Tnfa could interfere with the autophagy-mediated clearance of SVCV by host infected cells. ZF4 cells were incubated with Tnfa for 4 hours and autophagy levels were assessed by cellular LC3 distribution. Cells were treated with autophagy modulators, such as 3-Methyladenine (3MA) and rapamycin (Rapa) to respectively inhibit or enhance autophagy. As expected, autophagy (red puncta indicating L3C recruitment) was clearly diminished in 3MA-treated cells and, in contrast, strongly increased in Rapa-treated cells (both in number and size of the autophagosomes) (Fig 5A). Interestingly, Tnfa treatment

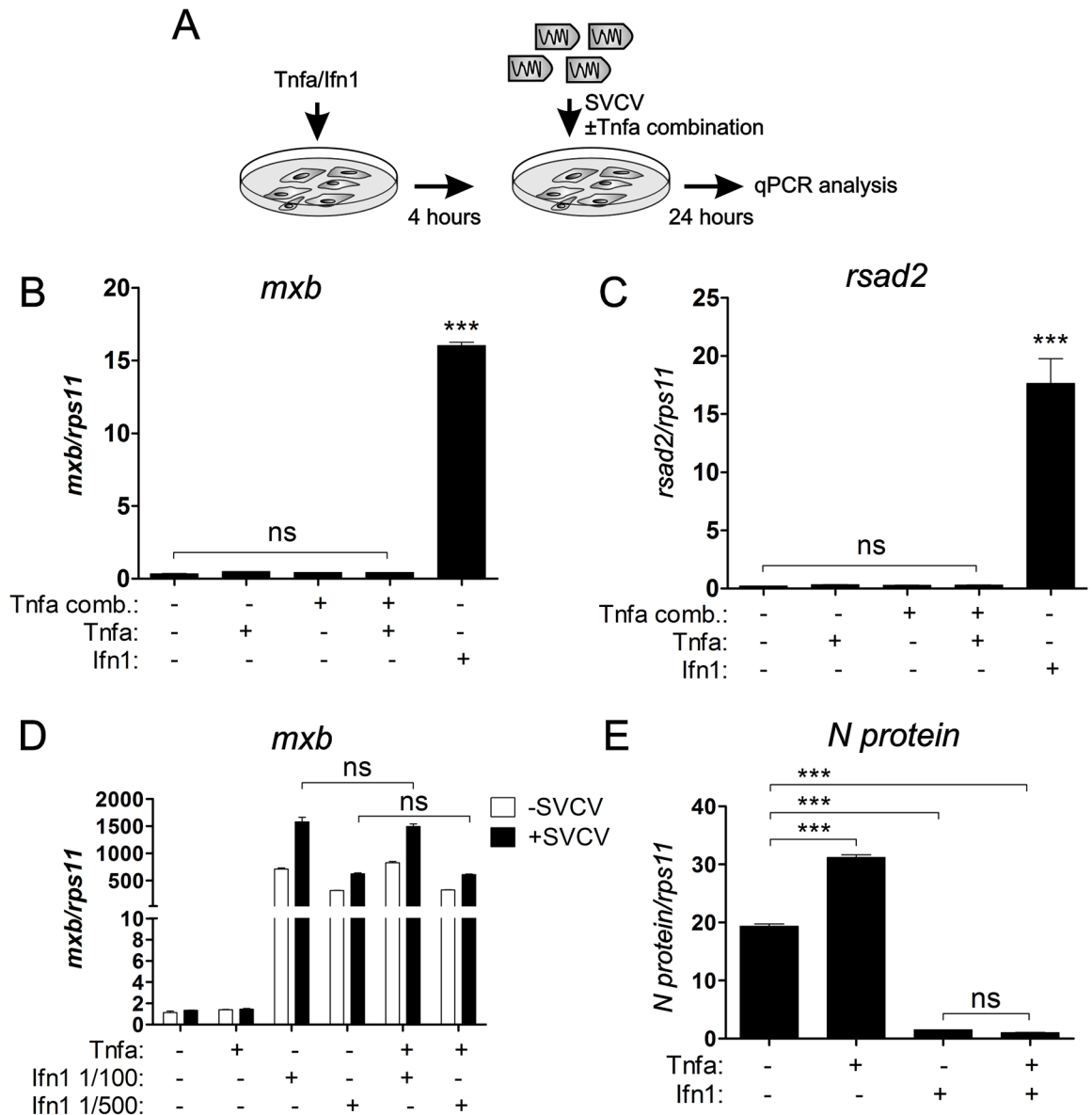


Fig 4. The antiviral role of interferon is not disrupted by Tnfa during SVCV infection. (A) Workflow representing the experimental design followed in (B-E). Briefly, Tnfa or Ifn1 were added to 80% confluent ZF4 cells and incubated for 4 hours. Subsequently, the medium was removed and fresh medium containing SVCV \pm Tnfa was added during 24 hours for the following qPCR analysis from mRNA extracted from the cell. (B, C) mRNA levels of the genes encoding for the antiviral genes *mxb* (B) and *rsad2* (C) of SVCV-infected ZF4 determined by qPCR. Gene expression is normalized against *rps11* and multiplied by 10^4 for *mxb* and 10^2 for *rsad2*. Bars represent mean \pm S.E.M. of triplicate readings from one sample and the data are representative of two independent experiments. (D) qPCR analysis of *mxb* expression levels in non infected or SVCV-infected cells previously treated with Tnfa or two different dilutions of Ifn1 (1/100 or 1/500). The gene expression is normalized against *rps11* and multiplied by 10^3 . Bars represent mean \pm S.E.M. of triplicate readings from one sample and the data are representative of two independent experiments. (E) qPCR analysis of the N protein expression levels in SVCV-infected ZF4 cells previously treated with Tnfa or Ifn1. The gene expression is normalized against *rps11* and multiplied by 10^5 . Bars represent mean \pm S.E.M. of triplicate readings from one sample and the data are representative of two independent experiments. *** $p < 0.001$. ns, non significant.

doi:10.1371/journal.ppat.1005699.g004

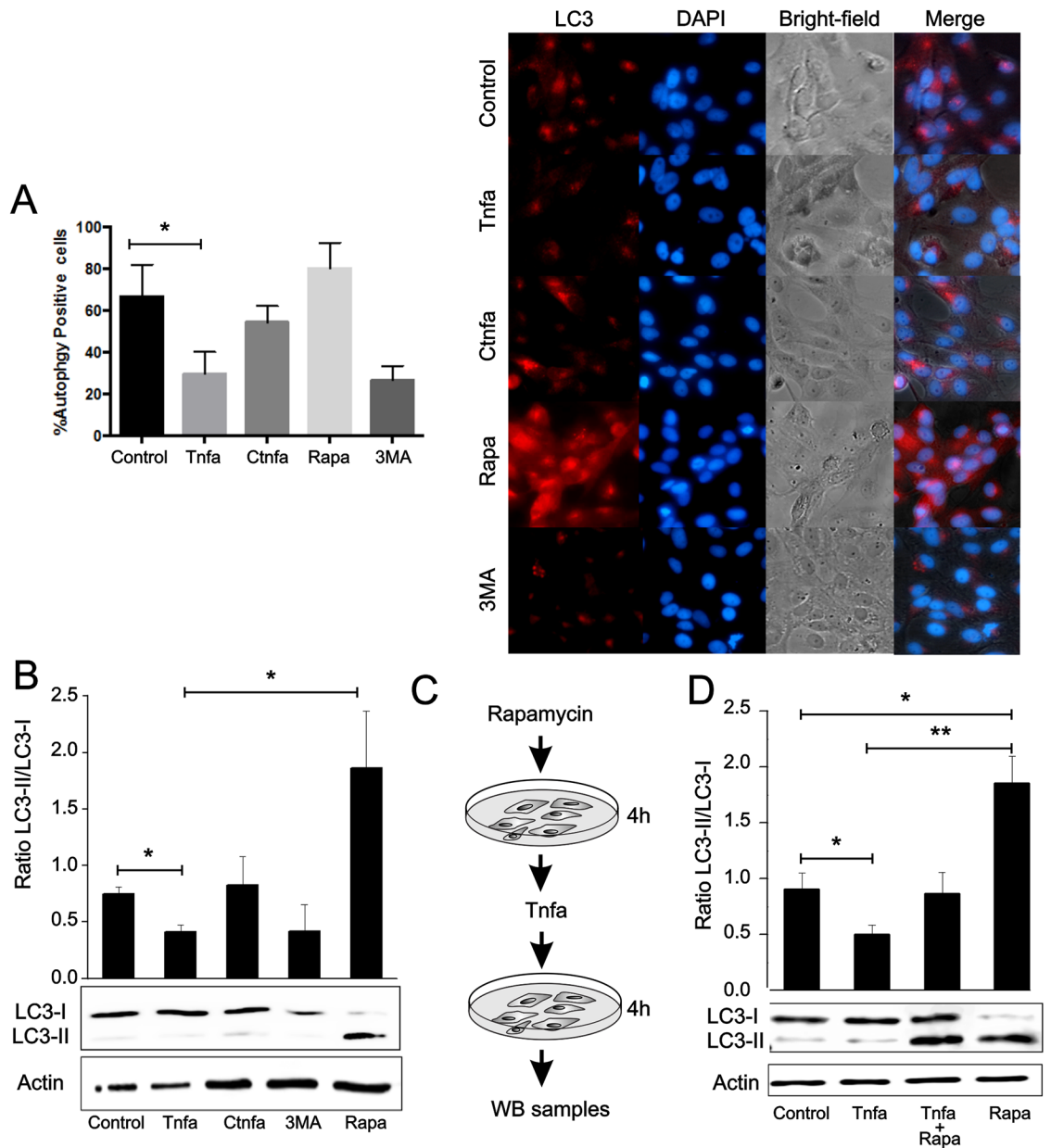


Fig 5. Tnf α inhibits autophagy. (A) ZF4 cells were treated with 0.1 μ g of Tnf α or inactivated Tnf α (CTnf α), 1 μ M of Rapa, 10 mM of 3-methyladenine (3MA) or remain untreated. After 4 hours cells were fixed and then incubated with an antibody anti-LC3. Cells were finally stained with a fluorophore-conjugated secondary antibody (red fluorescence, LC3) and DAPI (blue, cell nuclei). The number of cells with LC3 puncta ($n = 10$) was determined (left panel). Bars represent mean \pm S.E. M. Images are representative of the results obtained in 3 independent experiments (right panel). (B-D) Whole cell lysates were obtained from cells treated with Tnf α , CTnf α , Rapa or 3MA (B) or pre-treated with Rapa for 4 hours and then Tnf α or CTnf α was added for another 4 hours (C, D). LC3-I and LC3-II bands were visualized by WB using an anti-LC3 antibody and the protein content of the stained bands estimated by densitometry. The densitometry values were used to calculate LC3-II/LC3-I ratios. Actin bands were detected as a protein load internal control using an anti-actin antibody. Data are shown as the mean \pm S.E.M. of 3 independent experiments. * $p < 0.05$. ** $p < 0.01$.

doi:10.1371/journal.ppat.1005699.g005

diminished autophagosome formation suggesting that Tnfa inhibits autophagy (Fig 5A). In contrast, cells treated with heat-inactivated Tnfa (control Tnfa, CTnfa) did not affect autophagy (Fig 5A).

After autophagy induction, the cytosolic soluble form of LC3 (LC3-I) is conjugated to phosphatidylethanolamine to form LC3-phosphatidylethanolamine conjugate (LC3-II), which is recruited to autophagosomal membranes. This process is conserved among vertebrates and present in mammals [26] and in fish [25]. Therefore, LC3-II/LC3-I ratio is commonly used to quantify autophagosome formation by western-blot (WB) [27]. In order to quantify autophagy formation in Tnfa-treated cells, western-blot for LC3 was performed from lysates of Tnfa-treated ZF4 cells at 4 hours post-treatment (Fig 5B). The LC3-II/LC3-I ratio decreased by 2-fold in Tnfa-treated cells, but was unaltered in heat-inactivated Tnfa (CTnfa), indicating the negative impact of Tnfa in autophagy (Fig 5B). As expected, the LC3-II/LC3-I ratio decreased after 3MA treatment and increased after Rapa addition (Fig 5B). To further verify the Tnfa-mediated down-regulation of autophagy, ZF4 cells were pre-treated with Rapa for 4 hours and, subsequently, Tnfa was added for 4 hours and western-blot for LC3 was performed using the cell lysates (Fig 5C). The addition of Tnfa to Rapa-treated cells led to a 2-fold reduction in the autophagy activity compared to cells treated with Rapa alone (Fig 5D). As expected, incubation of Tnfa alone reduced the autophagy activity by 2-fold compared to untreated cells (Fig 5D). All together, these results indicate that Tnfa reduces autophagy in ZF4 cells. Moreover, these data suggest a role for Tnfa as a potent effector in reverting autophagy after this process has been initiated.

Tnfa impairs autophagy-mediated clearance of SVCV in ZF4 cells

We have previously demonstrated that autophagy has a protective role during SVCV and viral hemorrhagic septicemia virus (VHSV) infection [25]. To investigate whether Tnfa-mediated reduction of autophagy impairs SVCV clearance, ZF4 cells were pre-incubated with Tnfa prior to SVCV infection. As shown in the diagram of Fig 6A, the virus foci forming units (ffu) were first detected by immunofluorescence against N protein alone (Fig 6B), or in combination with LC3 (Fig 6D) or P62 (Fig 6E). To evaluate whether these ffu correlated with the infective viral particles, the SVCV present in the supernatant (viral yield) was also isolated and titrated by plaque forming units (PFU) (Fig 6A and 6C). The ffu number increased in Tnfa-treated cells compared to untreated and CTnfa-treated cells (Fig 6B). However, no differences on the foci size were found between these two treatments (Fig 6B). As expected, 3MA increased the ffu number, while Rapa decreased it (Fig 6B). Supernatant from cells treated with Tnfa contained 2.5-times more infective viral particles (4.5×10^5 pfu/ml) than un-treated (1.8×10^5 pfu/ml), or CTnfa-treated cells (1.4×10^5 pfu/ml) (Fig 6C). As expected, 3MA-treatment also increased the SVCV pfu/ml (5.5×10^5), while Rapa significantly decreased it (2.7×10^4 pfu/ml) (Fig 6C). Notably, although viral particles colocalization with LC3 and P62 puncta was hardly observed in control cells, probably reflecting the rapid degradation/loss of immunogenicity of the virus, it was nicely observed in cells treated with Tnfa (Fig 6D and 6E). Taken together, these results demonstrate that Tnfa impairs viral clearance through the inhibition of the autophagy response in infected cells.

Tnfa inhibits autophagy in vivo during SVCV infection in zebrafish larvae

To analyze the impact of Tnfa on the regulation of the host autophagic response to SVCV infection, we used a GFP-LC3 transgenic line that allows a real-time visualization of autophagy activity [28]. Morpholino-dependent Tnfa depletion resulted in increased basal autophagy in whole larvae, observed at low magnification as an increased fluorescence due to LC3

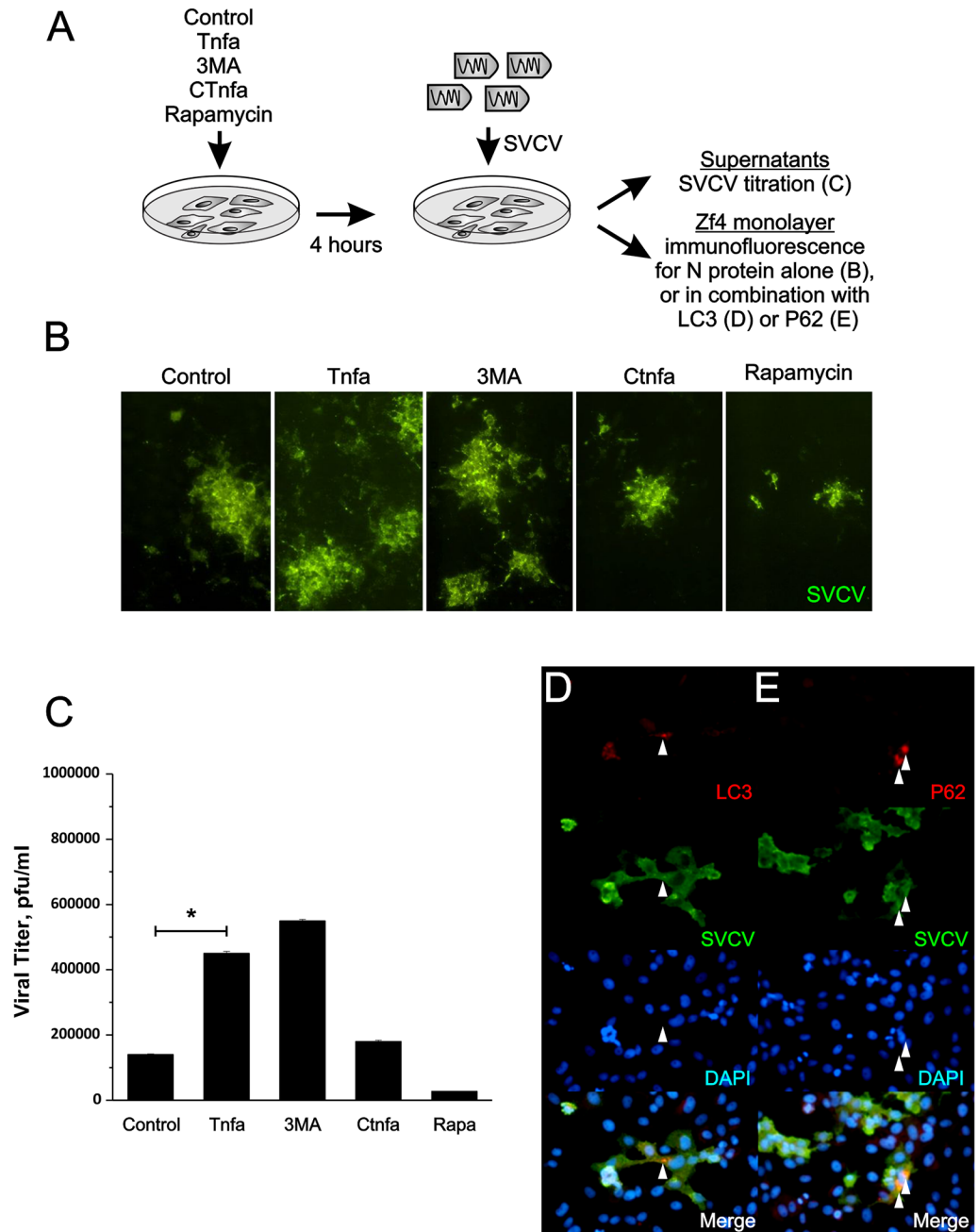


Fig 6. Tnfa increases the number of SVCV infective particles. (A) Workflow representing the experimental design followed in (B-E). Briefly, ZF4 monolayers were treated 0, 1 μ g Tnfa or CTnfa 1 μ M of Rapa, 10 mM of 3-methyladenine (3MA) or remain untreated (control) for 4 hours and subsequently infected with a m.o.i. of 10^{-2} for 4 hours. (B-E) After 24 hours of infection, cells were fixed and stained with anti-SVCV antibody followed by the incubation of a FITC-labeled secondary antibody alone or combined with anti-LC3 (D) or anti-P62 (E) antibodies followed by a CFTM594-labeled secondary antibody. (C) Virus titration in ZF4 cells in Plaque Forming Units per ml (PFU/ml) recovered from cell culture media of ZF4 pre-treated with Tnfa, CTnfa, 1 μ M of Rapa and 10 mM 3MA. Bars represent mean \pm S.E.M. of three independent experiments. * $p < 0.05$. (D,E) Colocalization of viral particles with autophagy markers (arrowheads) were observed and photographed with an inverted microscope.

doi:10.1371/journal.ppat.1005699.g006

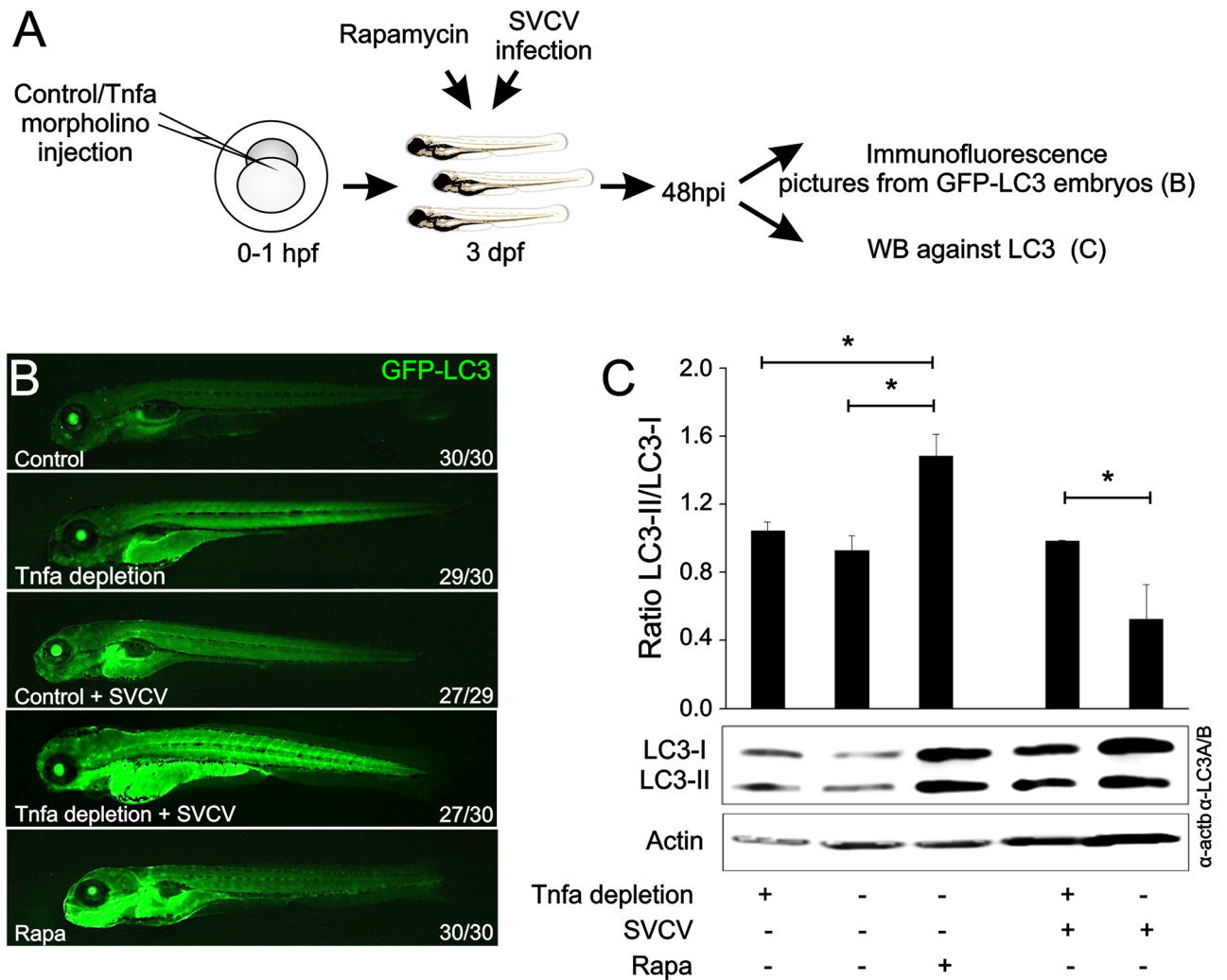


Fig 7. Tnfa inhibits the autophagy in zebrafish larvae. (A) Workflow representing the experimental design. (B) Zebrafish GFP-LC3 transgenic embryos were injected with Tnfa or Std mo at the one-cell-stage of development. After 48 hours, a group of larvae injected with Std-mo was immersed in a bath with 1 μ M Rapa and was freshly added every 24 h. The remaining larvae were divided in two and challenged by bath immersion with 10^9 TCID₅₀/ml SVCV or RPMI alone. After 72 hours of infection (5 dpf), larvae were collected, anesthetized with 0.16 mg/ml tricaine, mounted in 1% low melting point agarose supplemented with 0.16 mg/ml tricaine and images of the whole larvae taken using a Leica MZ16F fluorescence stereo microscope. Numbers in pictures represent the animals with the shown phenotype per total analyzed animals. (C) Zebrafish larvae were injected with morpholino (mo) Tnfa (Tnfa-MO) or Std (Std-mo) 1 hour post fertilization (hpf). After 36 hours, a group of larvae injected with Std-mo was immersed in a bath with Rapamycin and the remaining larvae (72 each group) were then divided in two and challenged by bath immersion with SVCV as above. After 48 hours of infection samples were recollected and LC3-I and LC3-II were detected by western-blot using an anti-LC3 antibody and the densitometry values were used to calculate LC3-II/ LC3-I ratios, represented as black bar graphs. Actin bands were detected as a protein load internal control using an anti-actin antibody. Data are shown as the mean \pm S.E.M. of 3 independent experiments. $p < 0.05$.

doi:10.1371/journal.ppat.1005699.g007

aggregation (Fig 7A and 7B). As expected, Rapa treatment also increased autophagy (Fig 7B). Moreover, as predicted from the previous *in vitro* data, SVCV-induced autophagy [25] was highly potentiated by depleting endogenous Tnfa [12](Lopez-Munoz et al., 2010)(Lopez-Munoz et al., 2010)(Lopez-Munoz et al., 2010)(Fig 7A and 7B). These results were confirmed by western blot analysis of the LC3-II/LC3-I ratio where depletion of Tnfa in infected larvae increased autophagy (Fig 7C). Therefore, Tnfa inhibits autophagosome formation during viral infection *in vivo*.

Discussion

Although the administration of anti-TNF α therapies normally aggravates viral infections, there are a few reports suggesting that TNF α inhibition could be beneficial for the treatment of certain viral infections [5]. However, the mechanism by which viruses manipulate the host-produced TNF α for their own benefit had never been determined. Here, we have used the zebrafish as an infection model to examine *in vitro* and *in vivo* the mechanisms by which TNF α enhances viral pathogenesis. We utilized the previously established viral infection model of SVCV in zebrafish, in which excess Tnfa had already been reported to increase viral susceptibility [9], to dissect the possible negative role of TNF α for the host during SVCV infection. Our studies demonstrate that Tnfa enhances SVCV replication through its receptor Tnfr2. Mechanistically, Tnfa does not alter SVCV binding to the cells, its escape from the endosome to the cytosol, or the Ifn-mediated antiviral response. In contrast, Tnfa inhibits autophagy both *in vitro* and *in vivo*, leading to decreased viral clearance and, consequently, to a higher susceptibility to the infection.

The increased survival of Tnfa- and Tnfr2-depleted larvae infected with SVCV demonstrates that Tnfa signaling through Tnfr2 has a deleterious effect in the host during SVCV infection. These results are further confirmed by the increased susceptibility of larvae forced to express Tnfa, confirming previous studies using recombinant Tnfa [9], and by the increased resistance of larvae forced to express a DN form of Tnfr2. The fact that the percentage of survival of Tnfr1-depleted larvae is slightly reduced compared to control larvae suggests that Tnfa signaling through Tnfr1 might have some protective role against SVCV infection. Furthermore, the observation that Tnfr2 depletion leads to a much higher larval survival than Tnfa depletion (70% versus 55%, respectively), further supports dual roles for Tnfa during viral infection, being protective signaling through Tnfr1 and detrimental signaling through Tnfr2. However, the overall effect of Tnfa during viral infection is predominately harmful for the host. Therefore, we need to be aware that the manipulation of each Tnf receptor leads to different outputs than Tnfa depletion alone. Thus, the use of specific TNF receptor inhibitors, rather than TNF α neutralizing drugs, could prove to be beneficial for the treatment of TNF α -related pathologies [15,29]. The potential protective role of signaling through Tnfr1 during SVCV infection still remains unexplored, and further experiments should be performed to investigate this phenomenon.

Since this is the first study conducted to address the enhancing role of TNF α in viral pathogenesis, we decided to dissect the essential steps occurring during viral infection in order to identify which of them, if any, were affected by TNF α . These steps include virus adherence to the cell, release from the endosome to the cytosol, replication and new viral particle formation. Our studies demonstrate that Tnfa slightly reduces SVCV binding to the ZF4 cells yet the fact that this modest reduction is also observed when Tnfa is added simultaneously with the SVCV, suggests that Tnfa could be physically interfering with the SVCV rather than deterring its adhesion through the TNF α activation pathway. In addition, we also demonstrate that Tnfa does not affect the SVCV capability to escape from the endosome to the cytosol.

Here, we have characterized the possible interference of TNF α in two key antiviral cell mechanisms that restrict virus replication: interferon response [30] and autophagy [31]. Our studies demonstrate that while Tnfa does not alter the interferon response during SVCV infection, it is able to diminish the viral-induced autophagic cell response *in vitro* and *in vivo*. Although TNF α has generally been linked to an up-regulation of autophagy [32–35], it has also been shown that, in certain contexts, TNF α up-regulates mTOR activity through NF- κ B, leading to autophagy inhibition [36]. In agreement with this, we provide evidences that Tnfa inhibits autophagy, which leads to increased viral susceptibility. Interesting, TNF α can also have a dual role in viral infection by promoting cell survival or cell death depending on the expression and activation balance of its receptors [37]. Although further studies should be conducted to

address whether the TNF α /TNFR2 axis indeed inhibits autophagy through the activation of NF- κ B, this is quite plausible since Tnfr2 mainly regulates NF- κ B activation in zebrafish larvae [15,29]. It would be of interest to inhibit TNF α , or potentially TNFR2, in SVCV-infected carps for the treatment of this viral disease that produces abundant losses in aquaculture worldwide. In addition, it would be advantageous to manipulate the activation of TNF receptors in those viral infections in which autophagy plays an antiviral role, such as HSV1, HIV-1, Sindbis virus, chikungunya virus and West Nile virus [38]. It is important to emphasize that anti-TNF α therapies have already been suggested to be helpful for the treatment of some of these aforementioned viral infections, such as HIV-1 [5]. This therapeutic approach could have important health implications for the treatment of these devastating viral infections since, to date, there are no available treatments for the majority of them.

Materials and Methods

Ethics statement

The experiments performed comply with the Guidelines of the European Union Council (86/609/EU) and the Spanish RD 53/2013. Experiments and procedures were performed as approved by the Bioethical Committee of the University of Murcia (approval number #537/2011).

Cell lines and virus

The fish cell line ZF4 (zebrafish embryonic fibroblast) was purchased from the American Type Culture Collection (ATCC, #CRL-2050). Cells were maintained at 28°C in a 5% CO₂ atmosphere in RPMI-1640 Dutch modified (Gibco) cell culture medium containing 10% fetal bovine serum (FBS) (Sigma, F6178), 1 mM pyruvate (Gibco), 2 mM L-glutamine (Gibco), 50 μ g/mL gentamicin (Gibco) and 2 μ g/mL fungizone (Gibco).

The SVCV isolate 56/70 (kindly provided by Dr. P. Fernández-Somalo, Laboratorio Central de Veterinaria, MAGRAMA) was propagated in ZF4 cells at 22°C as previously described [39]. Supernatants from SVCV-infected cell monolayers were clarified by centrifugation at 4,000 \times g for 30 min and kept in aliquots at -80°C. Clarified supernatants were used for the experiments. The virus stock was titrated in 96-well plates by limit-dilution (50% tissue culture infectious dose (TCID₅₀)/ml) [40].

Zebrafish husbandry

The zebrafish (*Danio rerio* H.) AB strain was obtained from the Zebrafish International Resource Center (ZIRC, <https://zebrafish.org/home/guide.php>). The transgenic line *Tg(CMV:EGFP-map1lc3b)^{zf155}* (GFP-LC3 for simplification) was previously described [28]. Fish were mated, staged, raised, and processed as previously described [41].

Morpholino and RNA injection and pharmacological treatments

In vitro-transcribed RNA of wild type Tnfa and DN Tnfr2 [15] was obtained following manufacturer's instructions (mMESSAGE mMACHINE kit, Ambion). Morpholinos were diluted in DEPC-treated water at a concentration of 0.3 mM (Standard-mo, Gene Tools) 0.5 mM (Tnfa-mo, 5'-GCAGGATTTTCACCTTATGGAGCGT-3' [42], 0.65 mM (Tnfr1-mo, 5'-ctgcattgtgacttactatcgac-3' [15], 0.3 mM (Tnfr2-mo, 5'-ggaatctgtgaacaaaggacaa-3' [15]. Morpholinos and RNA were mixed in microinjection buffer and microinjected into the yolk sac of one-cell-stage embryos using a microinjector (Narishige) (0.5–1 nl per embryo). The same amount of MOs and/or RNA were used in all experimental groups. The efficiency of the MOs was checked by RT-PCR [15,42].

In vivo viral infection assays

Groups of 20–40 wild type or GFP-LC3 transgenic zebrafish larvae of 3 days post fertilization (dpf) were challenged at 26°C by bath immersion in 5 ml of filtered egg water (60 mg/ml sea salts in distilled water) containing $\sim 10^9$ TCID₅₀ (50% tissue culture infectious dose)/ml SVCV. Twenty four hours later, the solution containing the larvae was diluted by adding 35 ml of egg water and the larvae were monitored every 24 hours for 8 days for clinical signs of disease and mortality. Fifteen pooled larvae were collected at 48 hpi in 250 μ l Trizol (15 larvae) for gene expression studies. For *in vivo* visualization of autophagy activity, GFP-LC3 transgenic larvae were anesthetized at 48 hpi (5 dpf) with 0.16 mg/ml tricaine and mounted in 1% low melting point agarose supplemented with 0.16 mg/ml tricaine. Images of the whole larvae were then taken using a Leica MZ16F fluorescence stereo microscope. As positive control, 48 hpf larvae were treated with 1 μ M Rapa (Calbiochem) for 72 h.

In vitro viral infection assays

The SVCV infectivity *in vitro* was evaluated by two different methods, RT-qPCR and foci forming unit assays. To detect SVCV by RT-qPCR, ZF4 cells were cultured in 25 cm² flasks at 80% confluence and treated with 100 ng/ml of zebrafish recombinant Tnfa [9] or Ifn1 (dilutions 1/100 or 1/500) [43] for 4 hours at 28°C and 5% CO₂. Subsequently, the media was removed, cells were washed twice with the cell media containing 2% FBS and infected with SVCV (multiplicity of infection (MOI) of 10^{-3}) in the presence or in absence of Tnfa (100 ng/ml) at 22°C for 24 hours. Afterward, the media was removed, RNA extracted, cDNA obtained and qPCR carried out as below indicated. Two different sets of primers (S1 Table) were used for SVCV detection: i) to quantify virus replication a primer pair amplifying the mRNA of N protein of SVCV and ii) to quantify the amount of viral genomes (negative sense RNA), a primer pair designed to detect the negative sense RNA encoding the gen of SVCV G protein.

For foci forming unit assays a previously developed methodology [44] with minor modifications was used. Briefly, ZF4 cells, grown on 96-well plates, were treated with 0.1 μ g/ml or 1 μ g/ml Tnfa, 1 μ g/ml heat inactivated (C Tnfa), 1 μ M RAP or 10 mM 3MA at 28°C for 4 hours. After incubation, cell culture medium was removed and cells were infected with SVCV (multiplicity of infection (MOI) of 10–2) at 22°C. Two hours post-infection, the supernatants from infected cell cultures were removed to eliminate non-bound virus, cell media containing 2% FBS added and plates further incubated for 24h. On the one hand, supernatants from infected cells were harvested and stored at -80°C for viral titration to determine the virus yield as below indicated. On the other hand, cell were fixed with a solution of 4% formaldehyde (Sigma, F1635) for 15 min, washed with PBS and further fixed with cold methanol (-20°C) for 15 min. Fixed cells were stained with a monoclonal antibody to SVCV (Teknokroma Analítica S.A. monoclonal antibody anti-SVCV) at 4°C for 24h [45]. After washing with PBS and cell monolayers were incubated with a FITC-labelled rabbit anti-mouse antibody (SIGMA) diluted 1/500 and incubation was continued for 30 min. Stained SVCV infected cell foci were then viewed and photographed with an inverted fluorescence microscope (Nikon Eclipse TE2000-U; Nikon Instruments, Inc., NY) provided with a digital camera (Nikon DS-1QM, Nikon Instruments, Inc., NY). At least, three different assays, each in duplicated, were performed

Viral yields

Virus titers in the supernatants of SVCV infected cells in the presence or absence of Tnfa were determined by a plaque forming units assay [39] and expressed as plaque forming units (PFU) per ml. Briefly, different dilutions of each supernatant (from 10^{-3} to 10^{-9}) were added to ZF4 cell monolayers, grown on 24-well plates at 22°C for 2 hours. Then, culture media was removed

and the infected cell monolayers covered with a solution of RPMI-1640 cell culture medium with 2% FCS and a 2% aqueous solution of methyl cellulose (Sigma). Cell plates were incubated at 22°C for 5 days and then the media with methyl cellulose was removed. Finally, wells were stained with crystal violet-formalin and plaques counted.

Viral binding assays

To analyze whether or not TNF α impairs the binding of SVCV viral particles to target cells, ZF4 cells grown in 25 cm² flasks at 80% confluence, were treated with TNF α (100 ng/ml) for 4 hours at 28°C. The media was then removed, cells were washed twice with the cell media containing 2% FBS and infected with SVCV (10⁻³ MOI) in the presence or absence of TNF α (100 ng/ml) for 30 minutes at 4°C to allow virus binding/attachment but not its endocytosis. Afterward, the media was removed, cells washed twice with cell media containing 2% FBS, RNA extracted and cDNA obtained. By means of qPCR using specific primers ([S1 Table](#)) the presence of SVCV G protein in the surface of the infected cells (viral binding) was evaluated.

Fusion assays

ZF4 cells, grown on 96 well-plates, infected with SVCV (MOI of 10⁻²). Two hours post-infection, the supernatants from infected cell cultures were removed to eliminate un-bound virus and fresh cell culture medium 2% FBS was added. After 24h of incubation at 22°C, the cell culture medium was removed and the SVCV-infected cell monolayer treated with Tnfa (100 ng/ml) for 45 min. The cells were then washed and the membrane fusion triggered by incubating the cells with fusion medium [44] at pH 6 for 30 min at 22°C. After that, cell monolayers were washed and subsequently incubated with fusion medium at pH 7.5 for 2 h at room temperature. Finally, cells were fixed with cold methanol (-20°C) for 15 min, dried and stained with Giemsa (5 mg/ml in PBS). Cells were viewed and photographed with an inverted fluorescence microscope (Nikon) provided with a digital camera (Nikon DS-1QM). At least, three different assays, each in duplicated, were performed.

Western blot

ZF4 cells were grown on 24-well plates in culture medium supplemented with 10% FBS at 28°C. After 24 h, the different treatments (1 μ M RAP, 10 mM 3MA, Tnfa (100 ng/ml) or CTnfa (100 ng/ml) were added. After 4 hours of incubation, culture media was removed and cell monolayers were resuspended in 500 μ l of PBS with a cocktail of protease inhibitors (Sigma). Cells were then processed to a frozen/thawed cycle 4 times and protein concentration adjusted before loading protein samples onto the gel. Samples were then loaded in Tris—Glycine sodium dodecyl sulfate 17% polyacrylamide gels under reducing conditions and the electrophoresis performed at 100 V for 90 min. The proteins in the gel were then transferred to nitrocellulose membranes (BioRad) for 75 min at 100 V in transfer buffer (2.5 mM Tris, 9 mM glycine, 20% methanol). The membranes were then blocked with 8% dry milk, 0.05% Tween-20 in PBS. Then, the membranes were incubated with the primary antibody microtubule-associated protein 1 light chain-3 (LC3)-I/LC3-II, a polyclonal antibody anti-LC3A/B (Cell Signaling Technology) diluted 1000-fold in PBS containing 5% BSA and 0.1% Tween-20 as indicated by the manufacturer. Membranes were then washed 3 times with PBS containing 0.05% Tween-20 for 15 min before incubation with GAR-Po in 0.5% milk in PBS for 90 min. After the last 3 washes with PBS containing 0.05% Tween-20, the peroxidase activity was detected by using ECL Select chemiluminescence reagents (Amersham Biosciences, RPN2232) and revealed by exposure to X-ray. Protein bands were analyzed by densitometry using the Totalab Software. Analysis of LC3-I and LC3-II bands was performed and calculated as relative to the

actin intensity band. Results are presented as the ratio of LC3-II/LC3-I from 3 independent experiments.

Immunofluorescence assays

After 4 hours of incubation with the different treatments (1 μ M RAP, 10 mM 3MA, Tnfa (100 ng/ml) or CTnfa), monolayers were fixed with a solution of 4% formaldehyde (Sigma) for 15 min, washed with PBS and further fixed with cold methanol (-20°C) for 15 min. Cell monolayers were then incubated overnight at 4°C with the anti-LC3 or anti-p62 (Abcam) antibodies in dilution buffer (PBS with 0.03% Triton X 100 [Sigma]) and 5% of albumin from bovine serum (BSA, Sigma). To visualize LC3 and p62, monolayers were washed again and incubated with appropriate secondary antibodies (in dilution buffer) for 1 h. To visualize nuclei, cells were stained with 1 $\mu\text{g}/\text{mL}$ of 4'-6-Diamidino-2-phenylindole (DAPI) for 10 min. Cell monolayers were finally washed for another 3 times. Cells were viewed and photographed with an inverted fluorescence microscope (Nikon Eclipse TE2000-U; Nikon Instruments, Inc., NY) provided with a digital camera (DS-1QM, Nikon Instruments, Inc., NY).

RNA isolation, cDNA synthesis and RT-qPCR assays

Total mRNA was extracted from pooled larvae or ZF4 cells with TRIzol Reagent (Life Technologies) and purified using the PureLink RNA Mini Kit (Life Technologies) following the manufacturer's instructions. Isolated RNAs were stored at -80°C until used. The purified mRNA was treated with DNase I, amplification grade (1 unit/ μg RNA; Invitrogen). SuperScript III RNase H- Reverse Transcriptase (Invitrogen) was used to synthesize the first strand of cDNA with an oligo-dT18 primer from 1 μg of total RNA at 50°C for 50 minutes. Real-time PCR was performed with an ABI PRISM 7500 instrument (Applied Biosystems) using SYBR Green PCR Core Reagents (Applied Biosystems). Reaction mixtures were incubated for 10 minutes at 95°C , followed by 40 cycles of 15 seconds at 95°C and 1 minute at 60°C , and finally by 15 seconds at 95°C , 1 minute 60°C and 15 seconds at 95°C . For each mRNA, gene expression was normalized to the ribosomal protein S11 (*rps11*) content in each sample using the Pfaffl method [46]. In all cases, the PCR was performed with triplicate samples and repeated with at least two independent samples. The primers used are shown in [S1 Table](#).

Statistical analysis

Data are shown as mean \pm SEM of at least three separate assays for gene expression experiments. Data were analyzed by ANOVA and a Tukey multiple range test to determine differences between groups, while the differences between two samples were analyzed by the Student t test. Log-rank (Mantel-Cox) Test was used for the survival curves.

Supporting Information

S1 Table. Primers used in this study. The gene symbols followed the Zebrafish Nomenclature Guidelines (http://zfin.org/zf_info/nomen.html). ENA, European Nucleotide Archive. (DOCX)

S1 Fig. Related to Figs 1 and 2. Validations of the loss- and gain-of-function experiments used in this study. (A, B and F-I) RT-PCR analysis of Tnfa (A, B) and Tnfr1 (F, G) and Tnfr2 (H, I) induced altered splicing of the *tnfa*, *tnfr1* and *tnfr2* transcripts, respectively at 3 dpf. The annealing of mos (solid lines), the primers used for the amplification (arrowheads) and the inframe premature stop codons (asterisks) are indicated. (A, B) A 740 bp product with an intact intron inserted between exons 1 and 2 of *tnfa* was only observed in samples injected with

Tnfa MO, while the same was absent from standard mo-injected fish. (F, G) A 540 bp product containing a deletion of the last 16 bp of exon 6 of *tnfr1* transcript was observed in samples injected with Tnfr1 MO, while it was absent from standard mo-injected fish. This deletion resulted in a predicted Tnfr1 protein lacking the signaling domain. (H, I) A 611 bp product containing a deletion of whole exon 2 of *tnfr2* transcript was observed in samples injected with Tnfr2 mo, while it was absent from standar mo-injected fish. This deletion resulted in a predicted Tnfr2 protein lacking most extracellular domain and the whole signaling domain. (C-E) RT-qPCR analysis of 2 dpf larvae forced to express Tnfa (C) and DN-Tnfr2 (D), and amplicon obtained for the housekeeping gene *actb* (E).

(TIF)

S2 Fig. Related to Fig 4: The antiviral role of interferon is not disrupted by Tnfa during SVCV infection. mRNA levels of genes encoding the antiviral genes *mxc* (A) and *pkz* (B) of SVCV-infected ZF4 cells pre-treated with Tnfa or Ifn1, or Tnfa treatment in combination (Tnfa comb.) to SVCV infection determined by qPCR. The gene expression is normalized against *rps11* and multiplied by 10^4 for *mxc* and 10^2 for *pkz*. Bars represent mean \pm S.E.M. of triplicate readings from one sample and the data are representative of two independent experiments. *** $p < 0.001$. ns, non significant.

(TIF)

Acknowledgments

We thank Inmaculada Fuentes and Pedro Martínez for technical assistance, SAI staff for tissue culture support, and Clyde A. Campbell for critical reading of the manuscript. This study is dedicated to the memory of Amparo Estepa whose enthusiasm for science was passed on to all of the people who had the luck of working with her.

Author Contributions

Conceived and designed the experiments: REP AML FJR AE VM. Performed the experiments: REP AML FJR ALM SDT SC DGM AF. Analyzed the data: REP AML FJR ALM SDT SC DGM AF JM AE VM. Wrote the paper: REP AML AE VM.

References

1. Rahman MM, McFadden G (2006) Modulation of tumor necrosis factor by microbial pathogens. *PLoS Pathog* 2: e4. PMID: [16518473](#)
2. Domm S, Cinatl J, Mrowietz U (2008) The impact of treatment with tumour necrosis factor-alpha antagonists on the course of chronic viral infections: a review of the literature. *Br J Dermatol* 159: 1217–1228. doi: [10.1111/j.1365-2133.2008.08851.x](#) PMID: [18945310](#)
3. Ali T, Kaitha S, Mahmood S, Ftesi A, Stone J, et al. (2013) Clinical use of anti-TNF therapy and increased risk of infections. *Drug Healthc Patient Saf* 5: 79–99. doi: [10.2147/DHPS.S28801](#) PMID: [23569399](#)
4. Herbein G, O'Brien WA (2000) Tumor necrosis factor (TNF)-alpha and TNF receptors in viral pathogenesis. *Proc Soc Exp Biol Med* 223: 241–257. PMID: [10719836](#)
5. Kumar A, Abbas W, Herbein G (2013) TNF and TNF receptor superfamily members in HIV infection: new cellular targets for therapy?. *Mediators Inflamm* 2013: 484378. doi: [10.1155/2013/484378](#) PMID: [24453421](#)
6. Haraguchi S, Day NK, Kamchaisatian W, Beigier-Pompadre M, Stenger S, et al. (2006) LMP-420, a small-molecule inhibitor of TNF-alpha, reduces replication of HIV-1 and Mycobacterium tuberculosis in human cells. *AIDS Res Ther* 3: 8. PMID: [16573838](#)
7. Calabrese LH, Zein N, Vassilopoulos D (2004) Safety of antitumour necrosis factor (anti-TNF) therapy in patients with chronic viral infections: hepatitis C, hepatitis B, and HIV infection. *Ann Rheum Dis* 63 Suppl 2: ii18–ii24. PMID: [15479865](#)

30. Grandvaux N, tenOever BR, Servant MJ, Hiscott J (2002) The interferon antiviral response: from viral invasion to evasion. *Curr Opin Infect Dis* 15: 259–267. PMID: [12015460](#)
31. Deretic V (2005) Autophagy in innate and adaptive immunity. *Trends Immunol* 26: 523–528. PMID: [16099218](#)
32. Harris J (2011) Autophagy and cytokines. *Cytokine* 56: 140–144. doi: [10.1016/j.cyto.2011.08.022](#) PMID: [21889357](#)
33. Keller CW, Fokken C, Turville SG, Lunemann A, Schmidt J, et al. (2011) TNF-alpha induces macroautophagy and regulates MHC class II expression in human skeletal muscle cells. *J Biol Chem* 286: 3970–3980. doi: [10.1074/jbc.M110.159392](#) PMID: [20980264](#)
34. Jia G, Cheng G, Gangahar DM, Agrawal DK (2006) Insulin-like growth factor-1 and TNF-alpha regulate autophagy through c-jun N-terminal kinase and Akt pathways in human atherosclerotic vascular smooth cells. *Immunol Cell Biol* 84: 448–454. PMID: [16942488](#)
35. Lin NY, Beyer C, Giessel A, Kireva T, Scholtyssek C, et al. (2013) Autophagy regulates TNFalpha-mediated joint destruction in experimental arthritis. *Ann Rheum Dis* 72: 761–768. doi: [10.1136/annrheumdis-2012-201671](#) PMID: [22975756](#)
36. Djavaheri-Mergny M, Amelotti M, Mathieu J, Besancon F, Bauvy C, et al. (2006) NF-kappaB activation represses tumor necrosis factor-alpha-induced autophagy. *J Biol Chem* 281: 30373–30382. PMID: [16857678](#)
37. Aggarwal BB (2003) Signalling pathways of the TNF superfamily: a double-edged sword. *Nat Rev Immunol* 3: 745–756. PMID: [12949498](#)
38. Dong X, Levine B (2013) Autophagy and viruses: adversaries or allies? *J Innate Immun* 5: 480–493. doi: [10.1159/000346388](#) PMID: [23391695](#)
39. Garcia-Valtanen P, Martinez-Lopez A, Ortega-Villaizan M, Perez L, Coll JM, et al. (2014) In addition to its antiviral and immunomodulatory properties, the zebrafish beta-defensin 2 (zfBD2) is a potent viral DNA vaccine molecular adjuvant. *Antiviral Res* 101: 136–147. doi: [10.1016/j.antiviral.2013.11.009](#) PMID: [24286781](#)
40. Reed LJ, Muench H (1938) A simple method of estimating fifty percent endpoints. *Am J Hygiene*: 493–497.
41. Westerfield M (2000) *The Zebrafish Book. A Guide for the Laboratory Use of Zebrafish Danio* (Brachydanio rerio)*. Eugene, OR.: University of Oregon Press.
42. Lopez-Munoz A, Sepulcre MP, Roca FJ, Figueras A, Meseguer J, et al. (2011) Evolutionary conserved pro-inflammatory and antigen presentation functions of zebrafish IFN γ revealed by transcriptomic and functional analysis. *Mol Immunol* 48: 1073–1083. doi: [10.1016/j.molimm.2011.01.015](#) PMID: [21354627](#)
43. Lopez-Munoz A, Roca FJ, Meseguer J, Mulero V (2009) New insights into the evolution of IFNs: zebrafish group II IFNs induce a rapid and transient expression of IFN-dependent genes and display powerful antiviral activities. *J Immunol* 182: 3440–3449. doi: [10.4049/jimmunol.0802528](#) PMID: [19265122](#)
44. Mas V, Perez L, Encinar JA, Pastor MT, Rocha A, et al. (2002) Salmonid viral haemorrhagic septicaemia virus: fusion-related enhancement of virus infectivity by peptides derived from viral glycoprotein G or a combinatorial library. *J Gen Virol* 83: 2671–2681. PMID: [12388802](#)
45. Martinez-Lopez A, Garcia-Valtanen P, Ortega-Villaizan M, Chico V, Gomez-Casado E, et al. (2014) VHSV G glycoprotein major determinants implicated in triggering the host type I IFN antiviral response as DNA vaccine molecular adjuvants. *Vaccine* 32: 6012–6019. doi: [10.1016/j.vaccine.2014.07.111](#) PMID: [25203447](#)
46. Pfaffl MW (2001) A new mathematical model for relative quantification in real-time RT-PCR. *Nucleic Acids Res* 29: e45. PMID: [11328886](#)